Inferring Changes in Daily Human Activity from Internet Response

Xiao Song
University of Southern California
Information Sciences Institute
Los Angeles, United States
songxiao@usc.edu

Guillermo Baltra
University of Southern California
Information Sciences Institute
Los Angeles, United States
baltra@usc.edu

John Heidemann
University of Southern California
Information Sciences Institute
Los Angeles, United States
johnh@isi.edu

ABSTRACT

Network traffic is often diurnal, with some networks peaking during the workday and many homes during evening streaming hours. Monitoring systems consider diurnal trends for capacity planning and anomaly detection. In this paper, we reverse this inference and use *diurnal network trends and their absence to infer human activity*. We draw on existing and new ICMP echo-request scans of more than 5.2M /24 IPv4 networks to identify diurnal trends in IP address responsiveness. Some of these networks are *change-sensitive*, with diurnal patterns correlating with human activity. We develop algorithms to clean this data, extract underlying trends from diurnal and weekly fluctuation, and detect changes in that activity. Although firewalls hide many networks, and Network Address Translation often hides human trends, we show about 168k to 330k (3.3–6.4% of the 5.2M) /24 IPv4 networks are change-sensitive. These blocks are spread globally, representing some of the most active 60% of $2 \times 2°$ geographic gridcells, regions that include 98.5% of ping-responsive blocks. Finally, we detect interesting changes in human activity. Reusing existing data allows our new algorithm to identify changes, such as Work-from-Home due to the global reaction to the emergence of Covid-19 in 2020. We also see other changes in human activity, such as national holidays and government-mandated curfews. This ability to detect trends in human activity from the Internet data provides a new ability to understand our world, complementing other sources of public information such as news reports and wastewater virus observation.

CCS CONCEPTS

• **Networks** → **Network measurement**; **End nodes**; **Topology analysis and generation**.

KEYWORDS

Active Measurement; Diurnal Use; Internet Edge

1 INTRODUCTION

Humans are a major source of activity on the Internet—diurnal effects in network traffic have been observed since early telephone networks and are prominent in wired [58] and wireless networks [81, 96]. Traffic models consider diurnal trends during network provisioning [34, 48] and for anomaly detection [61]. Diurnal trends in traffic volume also appear in IP address usage [72] and must be accounted for in Internet outage detection systems [7, 45, 72, 74]. These systems detect changes in network activity (long-term traffic demand, network anomalies, outages) and factor out the diurnal trends caused by humans as a confounding signal.

We suggest the opposite inference can also be important: *detecting diurnal human activity from network observations, then using such activity to infer changes in human activity*.

Our work was sparked by the Covid-19 pandemic, where over a few weeks in 2020, millions of people shifted to work-from-home (WFH). Ongoing measurements revealed changes in our university's network usage that directly reflected this shift. Also, many researchers reported changes in network traffic, from increases in wired network traffic [55], and a 15–20% increase in IXP traffic [32]. In some cases, concerns about growth in streaming media prompted preemptive reductions in video quality [13]. Facebook reported a sharp 20% increase in traffic in late March after widespread WFH [11]. Mobile (cellular) networks showed a 25% drop in traffic and decreased user mobility as people stay at home [59]. The signal we are examining is how many IP addresses are active, and rather than using it to report on Internet use, we *invert* it to detect diurnal human activity, then look for *changes* in that activity. Our work provides global coverages without special access to traffic metrics (volume, latency, and availability, etc.)

Looking for changes in the diurnal network to infer human activity can be helpful for several reasons. External evidence of changes in human activity can help reduce uncertainty around public responses to large events, such as the global Covid-19 pandemic and regional protests. Evaluation of WFH in 2020 is useful to provide a view of states policies during this period, since news about WFH is not always widely available internationally, and it can be helpful to compare observed behavior to stated policy (for example, [31]). Beyond Covid-19 WFH, our approach can detect other changes in human diurnal activity. We have seen changes that correspond to public lockdowns in response to protests (see §4.3), for example. Our inference of human activity can be an independent viewpoint to illustrate responses to public policies, and to provide data in policy decisions.

Our work uses frequent pings (ICMP echo request) of the public IPv4 address space to observe diurnal network trends. As an

active measurement, this source has the advantage of providing a global picture, and pre-existing measurement activity provide data that covers the unexpected onset of Covid-19. A disadvantage of active measurement is that it cannot see behind widely used network address-translation in home routers, nor firewalls (as with prior work [71, 79]). We define change-responsive networks as those where diurnal human activity is strong enough to detect changes. We prove 168k to 330k blocks are suitable for activity detection (§3.4) globally (Table 2 and §3.5). These blocks can represent changes in human activity across 60% of $2 \times 2°$ geographic gridcells with networks. While "only" 60%, these are the most networked regions, and they represent 98.5% to 99.7% /24 blocks. Even in regions like North America and Europe, where always-on networking is commonplace, some change-responsive blocks indicate local human activity.

Our contribution is to be the first *to analyze network addresses to reveal the activity of human populations*. Prior work has used addresses to measure geographic events [69, 79], shown that they reflect ISP policies [14, 64, 68, 98], and human trends [25, 72, 81]. To our knowledge, we are the first to reverse this process and use addresses to infer human activity. We study only aggregate human activity; our approach respects individual privacy by focusing on /24 address blocks, and is IRB reviewed. We discuss research ethics in detail in Appendix A.

To evaluate human activity, we show how to interpret address responsiveness to indicate human activity, then detect changes in that activity in §2. This analysis requires several steps to clean the data, extract a signal from underlying trends, and detect changes in that signal (Table 1). We apply this new analysis to data from ongoing, active measurements of the Internet [71], and add new measurements to improve accuracy (§2.8). Re-analysis of existing data requires care, since ongoing measurements are optimized for other purposes, and its varying rate affects the accuracy for some blocks. Our additional measurements directly resolve these limitations. Our algorithm is inspired by observations where we had ground truth (Figure 1 and Appendix B). We support our design choices with systematic evaluation of our design decisions (§3.1 and §3.2).

The second contribution of our work is to show this signal provides global coverage and general correctness, even with pervasive Network Address Translation (NAT) and firewalls. Although we have data for more than 5.2M IPv4 /24 blocks, we see that about 168k to 330k (3.3–6.4% of the 5.2M) are change-sensitive. As we describe above, while this fraction is small, this one-in-twenty sample includes representative blocks for 60% of $2 \times 2°$ geographic gridcells with known IPv4 networks (Table 2 and §3.5). Such representatives help give insight into regional phenomena such as Covid-related health orders, and those change-sensitive blocks represent gridcells covering up to 98.5% of ping-responsive blocks. We validate coverage and accuracy in end-to-end comparison of detection in random /24 sample blocks (§3.6) and random locations (§3.7).

Focusing on human activity around the start of the Covid pandemic in early 2020 as prompting changes in human activity, we show that our algorithms detect network changes corresponding to Covid-WFH dates with high precision (93%, §3.6). Likewise, two randomly selected locations show network changes near their WFH dates (§3.7). High precision means we can confirm that detections

step	see	measurement risk	validation	coverage
Data import (active probing)	§2.2	firewalls, NAT, packet loss	[7, 71, 74]	5.2M blks.
(Opt.: addt'l observation)	§2.8	selecting right blocks	§3.2.3	1.8M blks.
Observation combination	§2.7	observer independence	§3.2.1	5.2M blks.
Address Reconstruction	§2.3	slow probing or rapid changes	§3.1	5.2M blks.
Change-sensitive blk. disc.	§2.4	NAT and servers	§3.2, §3.4	330k blks.
Trend extraction	§2.5	non-human-activity changes	[19, 80]	N/A
Change detection	§2.6	small or slow changes	[26, 47]	400k blks.
Change analysis	§2.6	multiple causes	§3.6	60% gridcells
		geolocation accuracy	§3.7	98.5% blks.

Table 1: Analysis and modeling steps from raw data to signal to detecting human-activity changes.

from our algorithm are human-related events. However, our recall is slightly lower (72%), showing that sometimes we detect events where we cannot identify clear root causes.

Our final contribution is to *use our algorithms and data to study the first six months of 2020*. We see significant changes in human activity throughout the world in 2020h1, as seen in Figure 8, corresponding to reactions to the Covid pandemic. In the end, we demonstrate the potential of our approach to *discover* Covid-related change found in the Philippines and India in Mar. 2020, and non-Covid-related change of Internet shutdown accompanied by curfews in India in Feb. 2020.

Data from our work is available at no cost [1], and we plan to release our analysis software with our paper publication.

2 METHODOLOGY

We infer changes in human activity from IPv4 address usage following the steps in Table 1. We begin by combining repeated pings of millions of blocks (groups of 256 adjacent IPv4 addresses), identify change-sensitive blocks reflecting diurnal human activity, and detect changes in use by block and geographic region.

Next, we illustrate this approach using an example shown in Figure 1. This block is at USC, so we know the start of WFH is on 2020-03-15, and that address changes we observe correspond to people at work. Our design considered manual examination of 2292 blocks, and we provide ground-truth examples in Appendix B.

2.1 Problem Statement and Challenges

We aim to identify human activity changes based on pings of millions of networks following the steps in Table 1. Our work was prompted by the desire to assess global reaction to Covid-19 WFH policies, but it can also detect changes in diurnal, human activity such as public holidays and political curfews. Our work can help identify or confirm such events, as shown in §4.

Our desire to detect changes in human diurnal activity has several motivations. Since our assessment uses public methodology and available data, it provides an independent, verifiable viewpoint. Even if coverage is incomplete (we certainly do not see all changes in activity!), independent evidence covering many locations can help assess reactions to public regulations, and provide insights in regions where public information is limited, incomplete, or distorted. We hope to complement existing public observations, particularly where information is sparse, confirming (Figure 9) and discovering events (Figure 10).

Challenges: Each step in our analysis (Table 1) faces risks and has been validated for correctness and completeness.

Dataset:	2019q4-w*	2020q1-w*	2020q2-w*	2020h1-w*	2020m1-w*	2020h1-ejnw *	2020m1-ejnw
duration (weeks)		12		24	4	24	4
completeness (sites)		1				4	
allocated blocks				14.5M			
not routed				3.3M			
routed blocks	11,095,220	11,121,592	11,149,787	11,149,787	11,121,592	11,149,787	11,121,592
not responsive	7,049,754	5,948,566	5,925,238	6,024,576	5,948,566	6,024,576	5,948,566
responsive	4,045,466	5,173,026	5,224,549	5,125,211	5,173,026	5,125,211	5,173,026
not diurnal	3,631,272	4,773,727	4,849,579	4,877,967	4,770,462	4,889,070	4,762,638
diurnal	414,194	399,299	374,970	247,244	402,564	236,141	410,388
narrow swing	1,375,566	2,145,246	1,700,045	2,269,473	2,951,412	1,825,465	1,641,216
wide swing	2,669,900	3,027,780	3,524,504	2,855,738	2,221,614	3,299,746	3,531810
not change-sensitive	3,675,118	4,855,201	4,948,888	4,956,244	4,863,004	4,937,024	4,840,113
change-sensitive	370,348	317,825	275,661	168,967	310,022	188,187	332,913

Table 2: Blocks before and after filtering (in /24s). Change-sensitive is interpreted as /24 blocks that are diurnal and with wide swing. Allocated addresses from IPv4 Address Space Registry [52]; Routing data from Routeviews [2–4].

Our ultimate test of correctness is an end-to-end evaluation focusing on known changes in human activity. To answer this question, we document changes that correspond with Covid-related events for two random graphic locations (§3.7). Working backward through our algorithm, we see good precision (93%) for randomly sampled blocks in §3.6. High precision shows our algorithm's results are almost always correct.

Our approach has representative blocks that are *near geographically complete*, covering 98.5% of the ping-responsive blocks, and 60% of all geographic regions. We directly observe changes in 168k to 330k network blocks (§3.4). While a small fraction of all the ping-responsive, public, IPv4 blocks (3.3–6.4% of 5.2M blocks in 2020), and *no active measurements* see behind NAT or firewalls that forbid probes, these blocks can represent events in the most populated geographic areas. Thus we *cover most places*, even though *we do not see everyone.* The geographic coverage and sample size, with our algorithm's high precision, provide useful results for most of the networked globe (§4), discovering events of which we are unaware.

To understand why our end-to-end evaluation is successful, we examine each step of our algorithm, validating what it models and potential sources of error (summarized in Table 1). Our work reinterprets existing datasets, so evaluation of data collection (and estimates of NAT and firewalls) are established work [7, 71, 74]. We use existing, proven algorithms for trend extraction [19, 80] and change detection [26, 47].

Analogies: We see our work as analogous to other non-traditional sources of epidemiology. In Covid-19 reporting, the "gold standard" for infection report is a PCR test administered by medical providers and reported through public health agencies. However, wastewater-based epidemiology [83] (WBE) estimates infection rates based on sampling virus DNA in sewage. WBE is necessarily imprecise about individuals and cannot detect infections from those using septic systems, but it provided early evaluation when testing was limited [63]. Similarly, researchers showed that influenza spread can be inferred from search queries in Google [38].

The ultimate benefit of our approach is to show that it is possible to interpret observations of Internet usage to infer information about the actions of the public, an approach to apply in future studies. In addition, we apply our approach retroactively to evaluate Covid-19.

2.2 Probing IP Addresses For Activity

Our approach leverages active probing of the IPv4 address space to monitor the status of addresses. Active probing allows us to observe if the target address is active or not, by reporting results as positive or non-replies.

We look for data that provides global coverage of address responsiveness, with data frequent enough to detect diurnal changes. We focus on source collecting data when Covid first spread in 2019 and 2020, in which we know people tend to change workplace to home. After examining several possibilities, we primarily use data from Trinocular, an Internet outage detection system operating since 2013.

We summarize prior detailed descriptions of collection [7, 71]: each of the six geographically distributed sites independently probes about 5.2M /24 IPv4 address blocks with ICMP echo request messages. Each site probes from 1 to 16 targets per block every 11 minutes, taken from a list with a pseudorandom order that is fixed for each quarter. Targets are limited to addresses that have ever responded to a complete scan in the last three years, written as $E(b)$. Probe rates are low enough that rate limiting is unlikely [46]. Although we consider data from all six sites, we discard two (sites c and g) in 2020 after identifying hardware problems that spoil the data. We merge data from the remaining sites (§2.3).

Sources Selection and Alternates: In principle, any frequent public scan of the IP space can serve as input.

We explored multiple alternative sources of active probing data. We compare our analysis to USC Internet surveys [49]. Surveys provide complete scans for selected blocks, (IP addresses every 11 minutes), but only for about 40k /24 blocks for about 4 weeks of every quarter, so the blocks are spatially and temporally incomplete. We use this data as ground truth for about 4k blocks in §3.2.1. We examined ZMap [28], with its quick, complete scans of IPv4, but it preserves only positive replies. Our algorithms require the timing of both positive and negative replies, and reconstruction of ZMap is impossible because it does not preserve probe order (or initial seed). Censys scans [27] emphasize daily services and certificates on hosts, not reachability many times per day, and bulk data is not
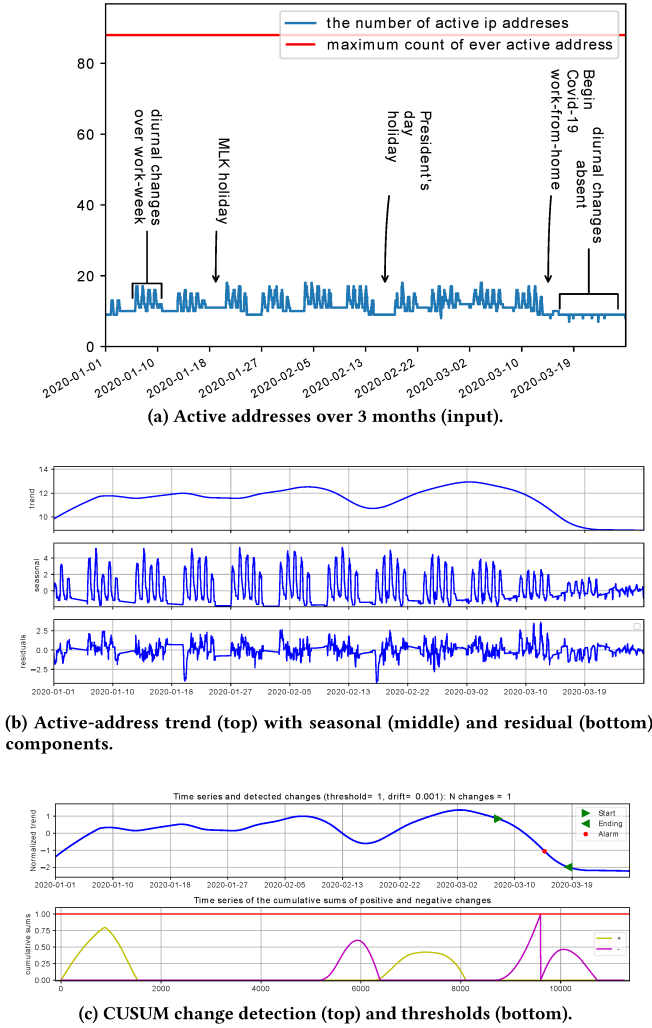
(a) Active addresses over 3 months (input).

(b) Active-address trend (top) with seasonal (middle) and residual (bottom) components.

(c) CUSUM change detection (top) and thresholds (bottom).

Figure 1: A block (128.9.144.0/24) illustrating address usage changes due to confirmed WFH.

round:	1	2	3	4	5	6	7	8	9	10
.1	**0**	0	0	0	**1**	1	1	1	1	1
.2	**0**	0	0	0	0	0	**1**	1	1	1
.3	**1**	1	1	1	**0**	0	**1**	1	1	1
.4	**1**	1	1	1	1	1	1	1	1	1
estimate:	—	**2**	2	2	**3**	**2**	**2**	**3**	**4**	4
truth:	**2**	2	2	2	2	2	**4**	4	4	4

Figure 2: Address reconstruction for a simple 4-address block over several rounds (changes in bold).

and n: Netherlands; w: Los Angeles). These sites provide very diverse perspectives, since each has different upstream ISPs, and they are on three continents. Although we consider data from all locations, we discard sites c and g in 2020 because of hardware problems. In the paper we use the term site and observer interchangeably.

IPv6: Our methods require seeing changes in address usage. These changes exist in IPv6, as seen by Google [41]. However, the IPv6's size and design prevent exhaustive probing [39, 40] and no IPv6 data is available to us. IPv6 address measurement is an active area of research [10, 35, 37, 66], and passive sources show promise for future IPv6 coverage [30].

2.3 Reconstructing Active Addresses

Our data source scans the visible Internet incrementally in rounds, so our first step is to reconstruct the state of the Internet from these incremental results.

Trinocular rounds occur every 11 minutes and probe 1 to 16 addresses. We ingest results incrementally to estimate how many are active. When all ever-active addresses ($E(b)$) have been observed, we have a complete *reconstruction* of the block. Then each subsequent round provides an adjusted estimate, updating prior data with any newly observed changes. Figure 2 shows 6 rounds of reconstruction in an artificial block. Scan rate (the light gray addresses) varies, and after one round with no output (scanning has not yet completed), the estimate is updated in rounds 2 and 5 to 8. Figure 1a shows active counts for a real block, where there are 88 probed addresses ($|E(b)|$, top red line), but only 8–18 are active during these three months (lower blue).

Accumulating state over multiple rounds leverages the fixed probing order (§2.2). We assume addresses do not change state until they are re-scanned, an assumption that holds if scanning is faster than addresses change. State changes (responsive to non-responsive, or vice versa) are due to laptop suspension or DHCP reassignment, both fairly slow [67]. The best case scan time for six observers scanning a 256-address block is 33 minutes (3 rounds), and the worst case is 8 hours (43 rounds, at one address per prober per round). The size of a complete block ($E(b)$) varies by history (updated each quarter), and the probe rate per round varies over the day based on responses (updated dynamically), so both bounds are atypical. In practice scan times are small (median: 2 hours, §3.1), and usually provide good accuracy (§3.2).

Mitigating probe loss: Address reconstruction is very sensitive to loss since a non-response to a query is interpreted as that address being inactive until the next time it is queried, and an observer will not retry until all other addresses have been scanned. Since queries are sent to unique addresses, spread out in time and space, queries that pass a congested link with loss rate p are reduced randomly by a factor of $(1 - p)$. When we combine observations from N

currently available. CAIDA's Archipelago [15] covers all routed /24 blocks, but it is far too slow to track diurnal trends. Its 3 teams of 17-18 probers cover all routed blocks every 2-3 days, about 1/256th the rate of Trinocular. Thus while these systems are tuned for their goals, none can be adapted to support diurnal analysis of most IPv4 or of 2020, although they may be extended for future use.

We also consider additional probing in §2.8 to improve coverage for some blocks. However, study of Covid-19's first spread necessarily uses only existing data. Reuse also avoids the small cost that active probing places on the world's networks, and avoids duplication of opt-out mechanisms and abuse handling, both operational costs of sustained probing.

Specific datasets: We list specific datasets covering October 2019 through June 2020 in an appendix (Table 6). This data is available at no cost to researchers. Trinocular collects data from six locations (coded c: Colorado; e: Washington, DC; g: Greece; j: Tokyo;

observers (later in §2.7), one congested observer will reduce address by $(1-p)/N$.

We apply *1-loss repair* to mitigate query loss. From [49] § 3.5, 1-loss repair examines queries to each address and replaces the pattern 101 (responsive, non-responsive, responsive) with 111, while ignoring 001, 110, and other patterns. This algorithm assumes the addresses are usually active for multiple probe rounds, so a better explanation for a single non-response is that the query (or response) was lost rather than the address was briefly unused. This algorithm assumes that active addresses are usually active for several probing rounds. The loss rate p is small, implying the probability of back-to-back query losses is very small (p^2). We show this algorithm has little effect on most blocks but correctly repairs the effects of one observer encountering loss on a congested link in §3.3.

We deployed 1-loss repair relatively late in our work based on evidence of congestive loss from one observer to a minority of destinations. Validated 1-loss repair is leveraged to address this problem with minimal changes to non-lossy links (§3.3). Complete counts (Table 2), coverage (Figure 7 and Figure 8) and all real-world results (§4) all employ 1-loss repair, but some preliminary results marked with an asterisk (*) use data without 1-loss repair. In validation of reconstruction (§3.2) and sample blocks (§3.6) we manually examined all the sample blocks to affirm sampled blocks did not see congestive loss from some observers. We are in the process of updating all results with 1-loss repair.

2.4 Identifying Change-Sensitive Blocks

To find changes in human activity, we need blocks that reflect people's daily schedules. We call such blocks *change-sensitive*, and identify them because first, they show a regular, *diurnal* pattern; second, the *swing* (high and low count) over 24 hours is large enough to detect its disappearance with confidence. We focus on change-sensitive blocks that show diurnal trends with a persistent daily swing to discard blocks that are inactive, occupied by always-on servers, and filtered by firewalls, since they are not change-sensitive.

Our example block (Figure 1a) is a known change-sensitive block. Active addresses over time (the blue line) usually show groups of five bumps, corresponding to the work-week, followed by two days of flat activity over the weekend. We also see known holidays on 2020-01-20 and -02-17.

Diurnal Blocks: We identify diurnal blocks by taking the FFT of the active addresses over time and looking for energy in frequencies corresponding to 24 hours, or harmonics of that frequency. This approach follows prior work [72], which shows that IP addresses often reflect diurnal activity, particularly in Asia, South America, and Eastern Europe.

Persistent Daily Swing: We look for blocks that have a "wide" daily swing in addresses, as described below. We define the daily swing as the range of addresses (maximum seen minus minimum) over midnight-to-midnight UTC.

A wide swing is a change of more than s addresses per day. Too large a threshold will reduce the number of accepted blocks, but too small makes the algorithm vulnerable to noise such as individual computer restarts. We select 5 as the minimum value that tolerates uncorrelated outages caused by a few computers (for example, due

to maintenance). The distribution of daily swing (omitted due to space) shows around 95% of blocks meet or exceed this threshold.

Finally, the swing must be *persistent* and reflects a *work week*. Changes need not occur every day, since many blocks (like Figure 1a) show use primarily during the work-week and not on weekends and holidays. We require blocks to have a wide daily swing for at least 4 of 7 consecutive days for at least one week in the observation period. We use a 7-day window since work activity usually follows weeks, and a 4-day minimum to tolerate 3-day weekends (for example, the week of 2020-01-20 in Figure 1a).

Coverage: Activity change detections show in change-sensitive blocks when diurnal changes disappear. We adopt Jan. 2020 as a baseline for what blocks are change sensitive; §3.4 shows that this provides good coverage (between 168k and 330k blocks meet these two requirements). Since it is before Covid was widespread it is not skewed by Covid-WFH. We ignore non-change-sensitive blocks since their operation (perhaps firewalls or NAT) hides human activity, as we discuss in §2.6.

2.5 Trend Extraction

The diurnal changes in our example (Figure 1) can be seen visually, however, in many blocks daily fluctuations make it difficult to detect changes in use. We expect changes will either remove the diurnal swing, as shown in Figure 1a after 2020-03-15, *or* decrease overall usage (and possibly the size of the swing), as fewer people come back to work. These signals are properties of the general baseline of active addresses and are obscured by daily changes and day-to-day variations, so we need to extract the trend from noise.

We track the underlying baseline by applying a standard seasonality model to the data. Seasonality models decompose the signal into a baseline convoluted with a daily and possibly weekly signal. We considered two models: the "naive" seasonality model [80] and Seasonal-Trend decomposition using LOESS (STL) [19, 80]. Although both are similar, we adopted the STL for our work after comparing the two and finding it more robust to outliers.

Figure 1b shows the decomposition from our sample block (Figure 1a) into trend, seasonal, and residual components. The seasonal component (middle) models daily and weekly changes, while the trend (top) captures the long-term mean value, and residual (bottom) shows any remaining error.

2.6 Detecting Changes in Usage

We detect changes by a sudden, large reduction of the diurnal pattern. Our sample block showed this signal, with diurnal activity before 2020-03-15 and flat activity being confirmed as laptops are now at home. This signal predicts human-activity changes and vice versa. We validate it with random studies (§3.6 and §3.7), events confirmed in public media (§4) and from network operators (Appendix B).

We automate the procedure with a standard change-point detection algorithm, CUSUM [26, 47] applied to the long-term trend in address usage. CUSUM flags upward or downward changes of the baseline, and the time of the largest change. Before applying CUSUM, we normalize the STL trend to its z-score (by subtracting the mean and dividing by the standard deviation), so we can use the same CUSUM parameters for every block (threshold: 1, drift: 0.001).

Figure 1c continues our example block showing CUSUM detection. The bottom graph shows the cumulative increase and decrease (in dark purple and light yellow). The upper graph shows the normalized trend with the start and end of the detected change as arrows on 2020-03-08 and -18. The point of change is 2020-03-15, which we confirm as to when WFH began. This change is detected from the fall in the normalized trend, reflecting the drop in address activity due to the absence of diurnal address usage (Figure 1a).

Geographic Aggregation: We geolocate all blocks (using Maxmind GeoLite [62]). Then we count blocks showing a decreasing trend (the purple line in Figure 1c) in each $2 \times 2°$ geographic region. (Two degrees is 222 km at the equator.) While IP geolocation has inaccuracies, using $2 \times 2°$ gridcells makes small inaccuracies less relevant, emphasizing expected city-level precision. Also, we discard gridcells with less than 5 change-sensitive blocks to avoid exaggerating visibility of changes in areas with little data, since such changes are less trustworthy. We focus downward changes in the long-term trend, since that reflects a reduction in the diurnal pattern, typically indicating an end to periodicity due to the work-week. Possible future work is to detect daily bumps and count how many occur to distinguish workplace networks from home networks.

Limitations and Other Sources of Change: CUSUM can automatically find activity indicating changes in change-sensitive blocks. In §3.6 we validate this claim, and §4 shows events we discovered with geographic aggregation. Changes in IP usage occur for many root causes, including user mobility, ISP renumbering, and network outages. An outage will be a downward change, followed by an upward change when the network recovers. Since outages are usually short (minutes or a few hours [45, 71, 74]), we identify and discard closely timed down and upward changes as outages. ISP-based renumbering (disruptions and anti-disruptions [74]) also shows up as closely-paired upward and downward changes that can be identified similarly. We can filter out such events by comparing them with outage detections.

Our approach to detecting human-activity changes only in change-sensitive blocks and cannot see changes behind firewalls or NAT. Our results will be less successful in countries where most individuals are behind always-on NAT devices, such as the U.S. and Western Europe. In other countries, ISP customers are behind CG-NAT, sometimes with multiple layers. Carrier-Grade NAT (CG-NAT) is widely used for mobile phones, and some wired ISPs [76]. Like home-based NAT, CG-NAT may hide diurnal trends, but CG-NAT strategies such as paired pooling may expose diurnal trends by allocating active individuals to public IP addresses. Mobile phone activity is also complicated by opportunistic Wi-Fi at home [59]. We show good geographic coverage in §3.5, but the complexities of NAT from prior studies [43, 57, 76] leave detection behind NAT and CG-NAT for future work.

The success of our approach depends on seeing some users in many locations, and it does not require seeing all users everywhere. We show that our approach provides broad coverage, we see 168k to 330k change-sensitive blocks (Table 2) in many countries (see §3.5).

Our incomplete but widespread coverage suggests that our results are best used to estimate *trends* and not absolute counts of individual choice.

2.7 Using Multiple Observers

We estimate network usage in §2.3 with observations from a single observer. However, we have data available from multiple observers in different geographic locations (§2.2). Each observer probes the same targets in the same order, but they start independently and run unsynchronized, so they are almost always out of phase with each other.

We combine observations from multiple observers to reduce the time required for scanning the full block and improve reconstruction accuracy as shown in §3.1 and §3.2.

Combining observations also increases our coverage as discussed in (§4). It reduces per-site bias by assuming all sites are independent and correctly operating. Observers are independent because they are in multiple, physically distant locations and use different upstream network providers. This independence is quantified in [8].

To evaluate the correct operation and confirm independence, we analyze each observer independently and compare their results against each other. This test identified data collection problems in two observers, c and g, prompting us to remove them from analysis for 2020m1. We confirmed that these sites had hardware or network problems.

2.8 Adding Additional Observations

Reusing existing data (§2.3) means some reconstructed blocks are under-observed. Beyond combining all observers (§2.7), we next describe deploying an additional observer designed specifically to cover previously under-observed blocks. Additional observations require two decisions: which blocks need additional observations, and how to observe.

Blocks that need additional observations are those with many addresses which always respond, because our existing data source (Trinocular) stops probing on the first positive response for the block, as mentioned in §2.3. We identify such blocks by the block refresh rate (§3.1), as estimated from each block's historical response rate and the number of addresses that will be scanned ($E(b)$ from §2.3).

Additional observations are taken by a designed observer, given a list of blocks that would be under-observed. This observer runs the standard Trinocular algorithm, but extends each round with up to four extra probes per round, even after a positive response. We adjust the number of additional probes based on the current observation rate to meet our goal. We then combine these additional observations with other observers as in §2.7. Together, aggregated observations will scan the worst-case block (256 addresses, all always responding) in 352 minutes, and these four complete scans per day allow detection of diurnal activity for all blocks.

In §3.2.3, we show this strategy identifies blocks that otherwise would have insufficient reconstruction. We have deployed additional probing; regrettably, it cannot be applied retroactively to our 2020 data.

2.9 Sharing the Results

Our detection results are available on our website [86], with Google-maps-style pan and zoom, as well as custom visualizations of time series and ISPs that change [87]. Our detection data is available to researchers at no cost [1].

3 VALIDATING DESIGN CHOICES

Next, we evaluate the algorithm design. We begin with design decisions: Do we track block states quickly enough to see diurnal changes? How accurate is the reconstruction? How many blocks do we see, and where are they? We then evaluate end-to-end results: Do detections and discoveries match reports of real-world human-activity changes?

3.1 Block Refresh Rate

We examine how quickly to complete scans of each /24 block, a *full block scan* (FBS). Prior work has suggested that sparsely occupied blocks are fully scanned in about two hours in the worst case [7], but it covered only the subset of all blocks which were intermittently responsive. Our new analysis here examines change-sensitive blocks, a different subset.

Specifically, prior work bounded FBS time as part of improving outage detection in sparse blocks (those with low response rates) [7]. It showed 3.1 hours (17 rounds) as an upper bound for scanning sparse blocks, based on 15 probes per round (a chosen design limit), over 11 minutes, and 256 addresses to cover in the block. A more general worst case will consider blocks where all 256 addresses always respond, so only one address is probed per round and a full scan requires 256 rounds (1.8 days). Such blocks are not identified as change-sensitive, but this rare worst-case suggests we need to look at block scanning duration empirically.

We show cumulative distributions of scan time for all change-sensitive blocks in 2020q1 in Figure 3. There are four cases: a single observer, then combined data from two, three, and four observers, from the bottom to the top respectively. About 65% of the change-sensitive blocks can be fully scanned in 6 hours or less (the left vertical dashed line), when data is combined from four observers. By contrast, 6 hours provides about 48% of blocks with one. Given 12 hours, 4 observers cover 78% of blocks, compared to 61% with one. This result shows that multiple observers are important to see most diurnal changes (§2.7), and additional observations are required to handle the tail of challenging blocks (§2.8).

3.2 Reconstruction Quality

Change sensitivity requires sufficient block reconstruction to detect diurnal changes and swings. To evaluate when and why reconstruction is sufficient, we next compare our reconstruction to ground truth from complete data. Our estimates of block refresh rates (§3.1) suggest bounds on what we can measure (a refresh rate of 24 hours is below the Nyquist rate and so cannot track diurnal changes), but observation and the underlying changes are both non-linear, as it provides a pessimistic bound.

We compare reconstruction against ground truth: Internet address surveys (2020it89-w in Table 6) scan all addresses in a block every 11 minutes for two weeks. Surveys cover about 2% of the responsive blocks in the IPv4 Internet; we find 32,437 blocks overlapped between surveys and our data. We show reconstruction of two blocks (representative of the 5,440) in Figure 4 (details in Appendix C).

3.2.1 Quantifying Reconstruction Success. We first evaluate the success of block reconstruction across all blocks with ground truth in Table 3. Two weeks of full survey data (2020it89-w) are defined

Dataset:	2020it89 -w*	2020q1 -w*	2020q1 -ejnw *	2020m1 -ejnw *	2020it89 -match- ejnw *
duration (weeks)	2	12	12	4	2
completeness (sites)	full	1		…4-site …	
			(*intersected with it89-w)		
responsive			32,437		
not diurnal	25,170	30,137	29,493	29,049	27,674
diurnal	7,257	2,300	2,944	3,388	4,763
narrow swing	15,104	12,597	11,112	11,112	11,112
wide swing	17,333	19,840	21,325	21,325	21,325
not change-sensit.	26,997	30,630	30,434	29,890	28,643
change-sensitive	5,440	1,807	2,003	2,547	3,794

Table 3: Validation data: counts of blocks overlapping from reconstruction and Internet surveys.

as ground truth (probing all addresses every 11 minutes). We intersect the data with four reconstruction options: one observer for a quarter (2020q1-w), four observers for a quarter (2020q1-ejnw), four observers for a month (2020m1-ejnw), and four observers for two weeks (2020it89-match-ejnw). We expect more observers to provide better quality reconstruction.

It shows that shorter observation detects more change-sensitive blocks: comparing 2020q1-ejnw to 2020m1-ejnw (3 vs. 1 months in columns 3 and 4), shows one month detects 2,547 change-sensitive blocks while three months reduces that to 2,003. Reducing the duration to 2 weeks (2020it89-match-ejnw) yields the most change-sensitive blocks, confirming this observation. In the first quarter of 2020, we speculate that these changes may be due to Covid.

Second, we see that data from four observers improves change-sensitive detection, confirming our design of combining data from multiple observers (§2.7). Comparing 2020q1-ejnw or 2020m1-ejnw (columns 3 and 4) to 2020q1-w (columns 2): with 4 × more observations, multiple sites allow better reconstruction of address usage over the day, and therefore more frequent detection of diurnal blocks (2,547 or 2,003 instead of only 1,807).

Overall, of the 5,440 change-sensitive blocks in the ground truth, the 4-observer, 2-week reconstruction discovers 3,794, 70% of truth. The main reason it misses blocks is that they do not appear to be diurnal in reconstruction, but a shorter duration and more observers improve reconstruction, as shown below.

3.2.2 Causes of Imperfect Reconstruction. To understand why shorter duration and combining multiple observers help, we next look at two components of change sensitivity: checks for diurnal activity and consistent swing. The middle rows of Table 3 show how many blocks pass each of these checks in blocks that are present in the ground truth (2020it89-w) and our four reconstruction options.

Duration of observation strongly affects diurnal detection: 2020m1-ejnw finds 3,388 diurnal blocks (47% of ground truth), but reconstruction within three months detect 2,944 or 2,300 (4 and one observer, finding 41% and 32% of ground truth). With the same duration that the survey data has, 2020it89-match-ejnw finds 4,763 diurnal blocks. This drop confirms that diurnal activity changed for some blocks throughout 2020q1 as we apply our strict requirements across a longer duration.

However, reconstruction increases the amount of swing: it finds 19.8k to 21.3k blocks with a wide swing compared to 17.3k in the ground truth (a 14% to 23% overestimate).
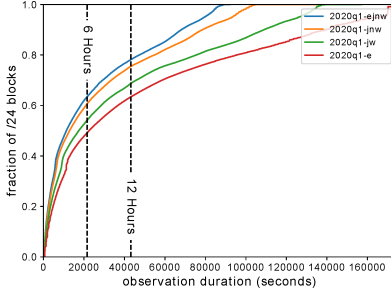
Figure 3: Cumulative distribution over all blocks of time to complete a scan of all known active addressees in 2020q1.
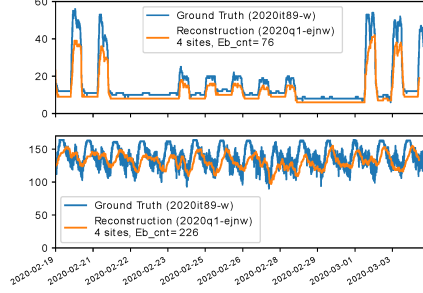

Figure 4: Comparing two reconstructed /24 blocks with their ground truth to show the similarities.
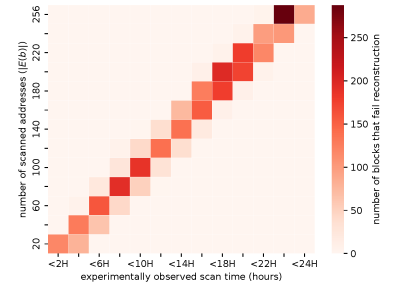

Figure 5: The count of change-sensitivity failures in reconstruction compared to ground truth.

These differences arise because reconstruction has fewer observations. Probing optimized for outage detection acts as a non-linear, low-pass filter over active addresses.

3.2.3 Additional probing to improve reconstruction quality. Reconstruction is challenged by insufficient data. We designed additional probing (§2.8) to fill this gap. We next explain that we can identify under-probed blocks (the tail of the distribution in Figure 3) to target additional probing.

Figure 5 shows the known change-sensitive blocks that are not classified as change-sensitive in reconstruction and so need improvement. This heatmap is grouped by scan time (x-axis) and scan size (y-axis). Problems occur in full blocks with longer scan time (away from the origin), although most blocks are near the origin.

Select Under-probed Blocks: We select blocks for additional probing by identifying those likely to be at the top right of these graphs. We model the expected FBS time with logistic regression parameterized by scanned addresses ($E(b)$, the y-axis of these graphs, defined in §2.2) and availability (A, the expected response rate of $E(b)$, defined in [71]), both of which we estimate from long-term data. Any blocks with an estimated FBS time of more than 6 hours are selected for additional probing, after discarding blocks with $E(b) < 32$ and $A < 0.05$, since they will always be near the origin. We select model parameters from experimentally observed FBS times of a random sample of 5k responsive blocks. The model is quite accurate, with only a 0.5% false-negative rate. Of our 5.2M responsive blocks, we select 1.8M for additional probing in 2022q2, and expect only 26k to be missed. We have deployed additional probing since 2022q3. Evaluating its performance in the real world is future work.

How Much Additional Probing: Given which blocks need additional probing, we must decide how much to probe. We know a full round must scan $|E(b)|$ in 6 h, or 32 11-minute rounds, so we require $|E(b)|/(6 \times 60/11)$ probes per round. We send at most one query to each block every 88 s (8 probes per round when $|E(b)| = 256$), half of our prior rate limit. This combination of existing probers and additional probing, guarantees that all blocks are scanned in at most 6 hours.

3.3 Mitigating Congestive Loss

The 1-Loss Repair algorithm (§2.3) is designed to mitigate the problem of one observer making observations through a link that encounters congestion. When congestion on the link is diurnal, it can falsely imply that addresses in the target block are used diurnally.

We discovered the presence of congestive loss when we found that additional observations (§2.8) *reduced* reconstruction quality. Additional information should only *improve* quality, but additional observations made over a link with congestive loss can reflect the state of the link instead of the destination's addresses. We use 1-loss repair to correct this problem.

We validate 1-loss repair based on examination of randomly selected 60 blocks, 40 were selected from two countries (China and Morocco) with many diurnal blocks, and 20 from other locations. Only two observers (w and sometimes c) show evidence of observation through lossy links for about one-quarter of Chinese destinations; we see only sporadic congestive loss for other observers in China and for any observer for other locations. Validation of these samples confirm that 1-loss repair corrects the effects of observations over links with up to moderate loss rates, and that it makes minimal changes to observers not observing congestive loss.

As one example showing this problem and recovery with 1-loss repair, Figure 6 examines one block. The charts show reconstruction from single observers (Figure 6a) and all observers without (Figure 6b) and with (Figure 6c) 1-loss repair. Each chart shows reconstruction for one quarter, with each address as a row and with time on the x-axis. Green horizontal lines are inferred address presence and gray is a non-response. Figure 6a shows reconstruction from single observers. Four observers (two on the top two charts, two others are omitted due to space) show consistent results, with each address active for multiple days (the long, green horizontal lines). However, observer w (the third chart from the top) shows congestion, with shorter green lines interrupted by gray. Quantitatively, Figure 6d shows that four observers see response rates with mean 0.620, but w sees 0.479, suggesting up to 14% loss. (This loss is overestimated due to Trinocular's outage-optimized sampling.) Congestive loss at observer w biases the all-observer reconstruction shown in Figure 6b, producing a response rate of only 0.581.

(a) Observers c and n (no congestive loss, top and middle) and w (with loss, bottom).

(b) Reconstruction from all 5 observers, *without* 1-loss repair.

(c) Reconstruction from all 5 observers, *with* 1-loss repair

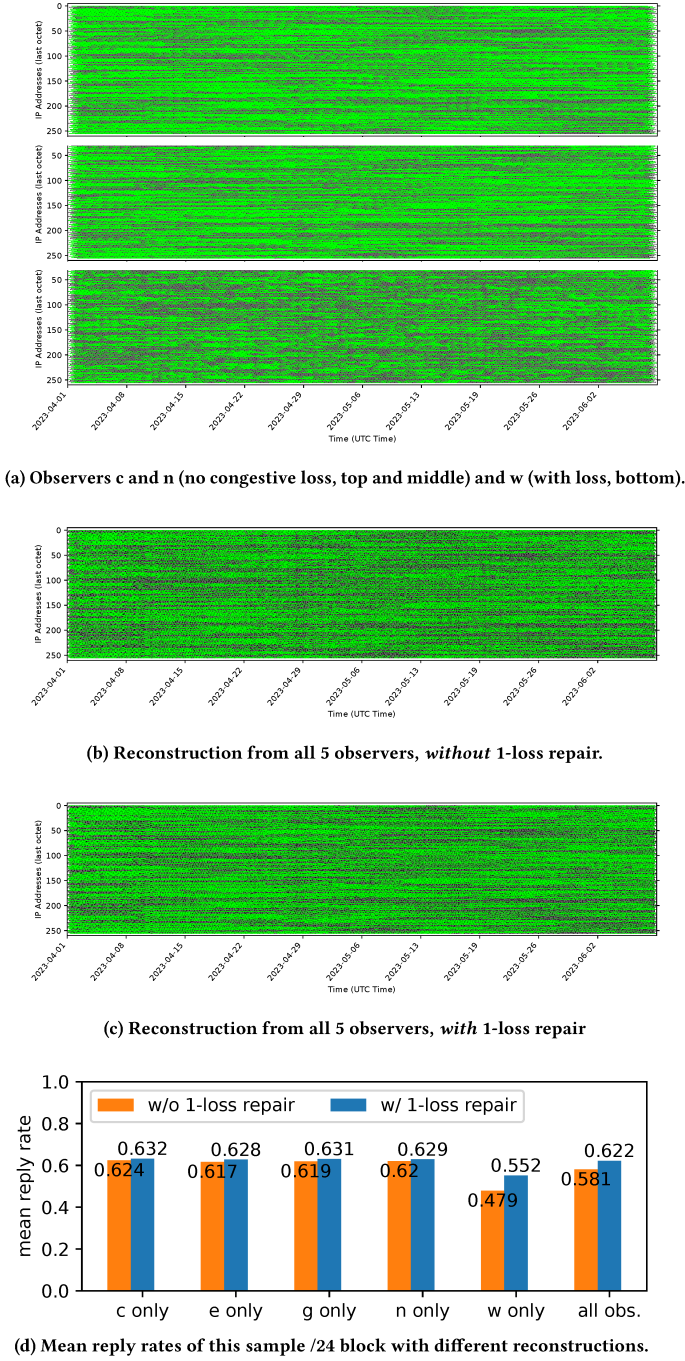**(d) Mean reply rates of this sample /24 block with different reconstructions.**

Figure 6: Reconstruction of a sample block: (a) observations from individual observers without and with congestive loss; reconstruction (b) without and (c) with 1-loss repair; and (d) reply rates for this block without and with 1-loss repair. Dataset: 2023q2.

Fortunately, 1-loss repair corrects random loss both for individual observers and the combined reconstruction. Figure 6d shows response rates for this block without (left bar of each pair in orange) and with (right darker blue bar) 1-loss repair. Reconstructions from individual observers without loss see minimal change (response rates increase by 0.010), while observer w changes from 0.479 to 0.552 (rising by 0.073). This improvement propagates to the all-observer reconstruction, where the 1-loss repair result of 0.622 is close to the non-lossy individual observers. Visually, we see that reconstruction with loss repair in Figure 6c is a better match to non-lossy single-site reconstructions in the top-two charts of Figure 6a than Figure 6b. We see similar results for most sample blocks with 1-loss repair [9], confirm its effectiveness and that all-observer reconstruction consistently provides the best reconstruction.

3.4 How Many Change-Sensitive Blocks?

We next explore how many change-sensitive blocks exist, how they change over time, and revisit the effect of observation duration on the number of change-sensitive blocks.

Decrease over Time: The left three columns of Table 2 show three quarters of data collected by one observer from 2019q4 to 2020q2. The number of change-sensitive blocks decreases somewhat over this period: from 370k to 327k to 275k. Some decreases from 2020q1 to 2020q2 may reflect Covid-19 WFH, as people move from universities and workplaces with more public IP addresses to homes where NAT hides status.

Churn: We see a fairly large rate of churn (turnover) in change-sensitive blocks. Comparing the first six months of 2020 (2020h1-w) with each three-month quarter (2020q1-w and 2020q2-w): the count for 2020h1-w is the intersection of the two quarters, and with 169k blocks, it is only 53% or 61% of each quarter. This drop is likely because our strict rules require consistent diurnality (§3.2.1). We see a similar drop to 189k when merging 2020q1-ejnw and 2020q2-ejnw, consistent with duration as the primary factor. Another possible reason for churn in the set of change-sensitive blocks in 2020 is the Covid-induced changes in network usage, as seen in §3.2.1.

Input Targets: A complicating factor in this analysis is that the underlying target list changes over time: in each quarter, the target list is updated to reflect currently responsive blocks, and in 2020m1 the target list was expanded from 4.0M blocks to 5.2M to take advantage of algorithm changes that correctly handle sparse blocks [7] (compare the number of responsive blocks in 2019q4-w and 2020q1-w).

Measurement Duration: We previously observed that longer periods decrease the number of diurnal blocks. We see that effect again here, comparing 2020m1-w to 2020q1-w and to 2020h1-w. As discussed in §3.2.1, to factor out this change, we detect change-sensitive blocks based on 2020m1-ejnw and apply that to all of 2020h1-ejnw for our data in §4. (The longer duration in 2020h1-ejnw would reduce the number of change-sensitive blocks by 45%, in part because of the very changes in address usage we are working to detect.)

Implications: Despite dynamics, we see 168k to 330k change-sensitive blocks, as shown in Table 2.

Any real-world system like the Internet will evolve, and the above factors of change of usage, churn, and new allocations all contribute to such non-stationarity. Non-stationarity is common

	gridcells		C-S blks-sum		ping-resp. blks-sum	
all	2,833		332.9k		5.17M	*100%*
under-observed	647				1K	*0.02%*
observed	2,186	100%	331.5k	*100%*		
under-represented	880	40%	1.1k	*0.3%*	70k	*1.3%*
represented	1,306	60%	330.4k	*99.7%*	5.1M	*98.5%*

Table 4: Geographic coverage of human-activity change detection, direct and block-weighted.

in measurement and can be addressed by regular retraining, as is already done for input targets. Our data shows coverage is sufficiently stable for the six months period we analyze here; we are exploring the integration of retraining in ongoing work.

3.5 Where are Change-Sensitive Blocks?

Prior analysis of diurnal blocks has shown their frequency varies by country [72]. Countries have different amounts of IPv4 address space. They also adopt different telecommunications and cultural policies about keeping devices "always-on". Change-sensitive blocks occur when devices are directly attached to the public Internet, so we do not see change-sensitive blocks in ISPs where devices use private address space behind an always-on router on the public IPv4 Internet. IP address assignment and use have been a topic of considerable study [14, 64, 67, 68, 72, 75, 76, 98]. Because of these variations in address use practice, the sensitivity of our approach varies by location, as we characterize below. A fuller exploration of the relationship between policy and change-sensitive blocks is future work.

Next, we summarize what we see. Figure 7 shows the locations of all change-sensitive blocks in 2020m1-ejnw. Circle area represents the number of change-sensitive blocks in each $2 \times 2°$ latitude/longitude gridcell.

The best coverage is in Asia, with moderate coverage in Europe and North America, and sparse coverage in South America and North Africa. Coverage reflects the intersection of where IPv4 addresses are allocated and where users of those addresses turn off devices at night. Moderate coverage from North America and Europe reflect widespread use of always-on home routers, which usually hide changes in end-user devices. (Although such routers use many public IPv4 addresses, their 24x7 operation means they are not diurnal or change-sensitive, and so their ping-responsiveness does not reveal periods of actual activity.) However, we do see diurnal blocks in North America and Europe at universities and in some ISPs where users occupy public IP addresses during the work-week (like Figure 1). The heavier presence in Asia is likely to reflect local ISP policies, with most users using dynamically assigned, public IPs. Future work could explore correlations of change-sensitivity with network types.

Coverage: To quantify the completeness of our geographic coverage, we evaluate how many gridcells can report human-activity changes. Our goal is to provide good coverage of represented areas of the globe, but we must define both "represented areas" and "coverage".

We consider a gridcell *represented* if it has at least 5 change-sensitive blocks, and *well-observed* if it has at least 5 ping-responsive blocks in our data sources. These thresholds allow us to compare

changes over several blocks, avoiding false positives due to noise in a single block. We evaluate sensitivity to different thresholds in Appendix D.

Table 4 reports all ping-responsive, geo-locatable IPv4 blocks. It evaluates coverage by the number of unique $2 \times 2°$ gridcells and by summing either change-sensitive or ping-responsive blocks in those cells.

It shows that we get reasonable geographic coverage: 60% of gridcells can be represented to report human-activity changes with the baseline of observed gridcells. While we miss 40% of gridcells, those we miss have very few users. We weigh coverage by the number of users in the second and third columns. We see that user-weighted coverage is very high: we can infer human-activity changes in gridcells for 99.7% of change-sensitive blocks and 98.5% of ping-responsive blocks from represented gridcells.

3.6 Validation by Sampled Blocks

We next validate the correctness of our algorithms by examining random samples, finding events in sample blocks, then looking for ground truth about that events in public news sources. In this section we validate for WFH early in the Covid pandemic, where changes in public health policies were widely adopted. We also recognize human-activity changes for other reasons, such as large public holidays (§4.2) and other government actions (§4.3). Here we focus on WFH because health policies are often publicly documented.

Defining correctness: We claim that changes in change-sensitive blocks can indicate human-activity changes, but defining "correct" can be challenging. Changes may occur for reasons other than human factors, such as suffering outages and shifting users due to maintenance. Also, our temporal precision is limited. We detect changes daily and must account for weekends, so detection may lag up to 4 days.

However, our goal is that our algorithms are *useful*, as case studies in §4 show. We quantify correctness in two ways to support that our algorithms should be trusted.

In this section, we evaluate random blocks, confirming they show CUSUM changes on dates that match confirmed WFH reports. We define block-level correctness as a WFH detection within four days of a public WFH report. This correctness is not as strong as the 1:1 mapping of events with WFH, but it suggests correlation. In §3.7 we examine random locations to see when groups of block-level changes correspond to WFH reports. We define location-level discoverability as a noticeable number of block-level changes corresponding to a public WFH report.

Together these metrics suggest utility.

Methodology: In Table 5, validation begins by selecting 50 random blocks from all change-sensitive blocks in 2020q1 (the first three months of 2020). This selection is unbiased and large enough to evaluate statistically. (Our case studies that examine locations (§4) are also helpful, but will under-represent blocks in urban areas.)

We then geolocate each block to match it to ground truth news reports. All blocks in our sample are geo-locatable. We see the blocks are global, in 18 different countries or regions, following the distribution seen in Figure 7, with 22 in China, 5 in Russia, 4 in Malaysia, 3 in India, 2 in Brazil and Hong Kong SAR (China), and the remaining 12 are single blocks in single countries.

Figure 7: The number of change-sensitive blocks (circle area) by geolocation (in a $2 \times 2°$ gridcell). Dataset: 2020m1.
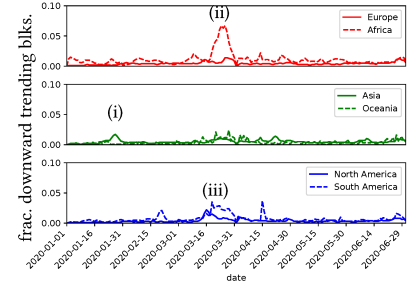

Figure 8: The human-activity changes for 2020h1 by continent.

dataset:	2020q1-ejnw
change-sensitive blocks	332,913
random selection	50
geo-locatable	50
no WFH in quarter	6
WFH in quarter	44
CUSUM near (±4d) WFH date	14
manual confirmation **(TP)**	13
apparent outage **(FP)**	1
no CUSUM near WFH date	30
visual-detection near WFH **(FN)**	5
CUSUM 5d from WFH	1
CUSUM not related to WFH	9
no CUSUM detections	15

Table 5: Validation of sampled blocks.

We then look at events per block and search for public news reports about Covid-19 lockdown dates. We use global Covid-19 lockdown dates from multiple media sources [6, 18, 20, 22, 36, 44, 54, 60, 65, 73, 85, 88–90, 92, 95]. Russian and Singapore lockdowns are not in this quarter (they are March 30 and April 7, but we cannot consider March 30 because of overlap with transients at the change of quarter), so we discard those 6 blocks, leaving 44 with news reports.

Correctness: For correctness, our algorithms detect changes in 14 of these 44 blocks. In 13 of those 14, we confirm a CUSUM-detected change in the raw data within 4 days of the reported Covid-19 lockdown date (true positives), showing *precision is 93%*—the detections that we see are usually Covid-related. A manual examination of raw data confirms these are real changes. The 14th block shows a change on 2020-03-21, during WFH—but the raw data suggests a network outage, not WFH. One of the remaining 13 shows a tiny visual change that are better detected by our algorithms, showing the importance of automatic, quantitative evaluation for accuracy. The other 12 all show WFH changes analogous to our example (Figure 1).

Completeness: While we do not claim a 1:1 association between detected changes and WFH events, we suggest *weak* completeness: do we detect all blocks that have changes? To determine all blocks with changes (positives), we manually examine 30 blocks without change in the WFH period for visual changes that are missed in CUSUM detection. We find 5 blocks (of 30) are missed by our algorithms but could have been found; these represent false negatives that we could find by tuning detection parameters. (The sixth block in China just misses our 4-day window, making it a true negative.) With 13 true positive detections in 18 positive events, that implies *recall is 72%* based on weak completeness.

Finally, 9 blocks show CUSUM detections at dates distant from WFH reports. Manual examination in raw data confirms these are real changes. They may be WFH that we could not document, some other human-activity changes in the region, or network maintenance actions like reassigning user IP addresses. We expect regional events to affect many people, so we can look for downward trends in other blocks in the same location, as we study in §3.7. The lack of other blocks with the same trend suggests network maintenance. We examined the locations of these 9 blocks, and only two had many other blocks triggering on the same day, suggesting two downtrend events that could not document as Covid-related and seven events consistent with small-scale network changes. This analysis suggests that correlated changes in one location are better predictors than the results of individual blocks.

3.7 Validation by Location

Examination of blocks suggests block-level precision is good, and our case studies (§4) suggest it can discover events. We next *validate* the ability of our algorithms to assist discovery, examining the data behind two random locations selected from all gridcells with change-sensitive blocks. As stated in §3.6, we focus on WFH as health policies are often publicly documented.

The United Arab Emirates: We randomly select gridcell (24N, 54E) in The United Arab Emirates and 25 of its 230 change-sensitive blocks. This country started a Covid-cleaning campaign on 2020-03-22 and began a night curfew on 2020-03-26 [21].

As before, we validate all blocks by comparing detection dates to news reports and examining raw data. Of the 25 blocks, 11 blocks have CUSUM-detected changes near the lockdown date. We confirm that all 11 blocks suggest Covid-related changes (true positives), showing *precision is 100%*. CUSUM changes peak on 2020-03-24 with 21.3% of blocks changing, ten times more than any other day in 2020h1. Four blocks show changes at other dates, but this huge peak focuses on the true WFH period. The other four blocks show changes in raw data but are not detected by CUSUM, suggesting 73% recall at this location.

Slovenia: We randomly selected The second gridcell (46N, 14E) in Slovenia. We examine 25 of the 936 change-sensitive blocks in the region. Slovenia closed all educational institutions on 2020-03-16, with additional suspensions later [84].

Of the 25 randomly selected blocks, we find 7 blocks show changes near 2020-03-16 and confirm them to be Covid-related (true positives), showing *precision is 100%*. The peak of changes on 2020-03-16 is larger than other peaks, supporting the 6 blocks showing non-correlated changes on other dates. Two blocks show changes in the raw data but are not detected by CUSUM, suggesting 77% recall here.

Discussion: These examples suggest that our approach finds outages at locations due to Covid. Enough blocks detect Covid-WFH to filter out non-correlated sources of change.

4 RESULTS: REAL WORLD EVENTS

In this section, we use our approach to discover real-world events related to human-activity changes and confirm them with ground truth. We report on trends in changes seen in 2020h1, and then present two case studies: China changes correlating with spring festival; and two curfews in India, the first pre-Covid and the second at the start of their Covid response.

4.1 Overall Trends

We next examine changes detected in human activity in 2020h1. Figure 8 shows the global count of downward trends in changes for each continent over six months. We geolocate blocks using Maxmind and assign each gridcell to a continent. By continent, data is heavily aggregated; we find data exploration is easier in a $2 \times 2°$ gridcell in our interactive website [86].

Although aggregated, we see several trends. First, the large percentage of changes in Asia around 2020-01-20 (at (i)) might correspond to the Spring Festival, celebrated widely in many Asian countries and regions. Most of the rest of the world showed significant changes around 2020-03-20 (at (ii) and (iii)), corresponding to initial Covid pandemic control measures. Low percentages in Oceania (dashed line, middle graph) show the success of their limits on international travel to control the spread of Covid in this period. The large percentage in Africa (at (ii)) reflects the over-representation of Morocco in our data (see Figure 7) and their lockdown beginning 2020-03-20 [50]. These trends show opportunities for global analysis; we next examine specific localities.

4.2 China in January

Here, we discuss the detection of activity changes in China in late January. We correlate these changes with two concurrent events: the Wuhan lockdown started on 2020-01-23 [6], and the week-long Spring Festival began on 2020-01-24.

Figure 9a shows downward network changes for all of China (in a $2 \times 2°$ gridcell) on 2020-01-27. We see large downward trends in several cities, including Wuhan.

For Wuhan's (30N, 114E) gridcell, Figure 9b illustrates the number of downward detections we observe for all blocks over six months. We see a peak in the first quarter around 2020-01-27, showing about 2.7% or 68 of 1,498 change-sensitive blocks reduce usage that day. We also see changes elsewhere in China at the same time, such as Shanghai (the light blue circle (30N, 120E) on the east coast of China, about 5.1% or 641 of 12,498 change-sensitive blocks) and
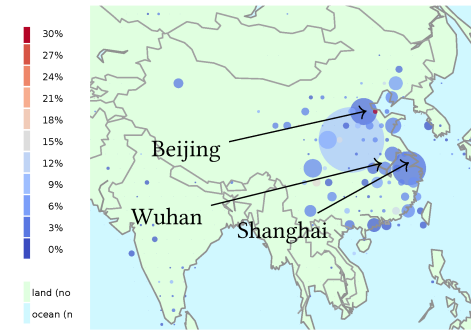
(a) $2 \times 2°$ gridcell map for 2020-01-27.
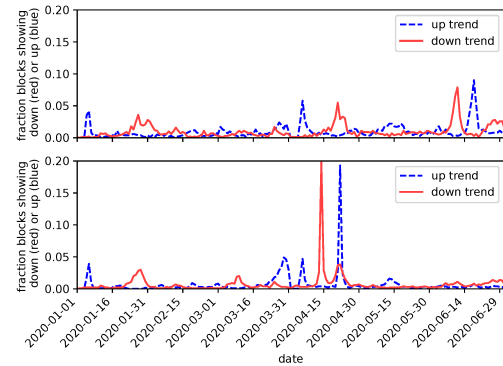
(b) Changes for (30N, 114E: Wuhan, top) and (38N, 116E: Beijing, bottom), 2020h1.

Figure 9: China

Beijing (another light-blue circle at (38N, 116E), about 3.5% or 402 of 11,412 change-sensitive blocks). Although a small percentage, both are large absolute changes.

Since the Wuhan lockdown and Spring Festival were concurrent events, we cannot attribute network changes specifically to either one. Our data confirm that we detected changes when Spring Festival began in China, and when Wuhan went into lockdown simultaneously, consistent with widespread media reports [6]. We again perform the same analysis on 2023q1, and observe similar changes during the Spring Festival Holiday, as shown in Appendix §B.3. However, we cannot determine if the Covid lockdown or Spring Festival solely caused the change in 2020.

In addition to the January peak matching spring festival, Figure 9b shows large peaks in April and June. We cannot find media reports of large events in these months. These events may be unpublicized or voluntary WFH, potential non-Covid events (described next), or possibly outages.

4.3 India in February and March

Our second case study examines India in February and March 2020. In browsing our data, we noticed hot spots of network changes starting on 2020-02-23 for several days. We observed that the east of New Delhi, where fewer networks made for a more significant relative change. As we refined our data processing, these changes were smaller than Covid-related lockdowns on 2020-03-23, but they
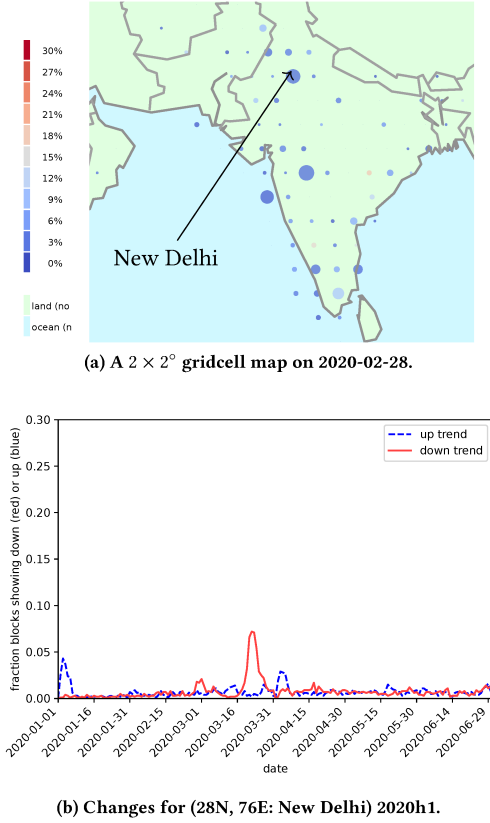
(a) A $2 \times 2°$ gridcell map on 2020-02-28.

(b) Changes for (28N, 76E: New Delhi) 2020h1.

Figure 10: India

provide evidence for network changes that are not Covid-related Figure 10a shows changes on the peak 2020-02-28, with a noticeable drop (2%, or 38 of 1,873 change-sensitive blocks) in usage, which correlates with riots over several days (-02-23 to -29) protesting changes in immigration law [91]. This location's largest drop (8%, or 151) occurred on 2020-03-22, which corresponds to the first Covid-related curfew in India: the Janata curfew on 2020-03-22 [54] and lockdown on 2020-03-24.

We have no evidence of curfews, but there were calls for curfews and police and army intervention, suggesting people chose to stay home. These examples of Covid-related WFH in March and non-Covid-WFH in February suggest that WFH can have multiple causes, but their outcome on the Internet is similar. We perform the same analysis for 2023q1, and observe no changes in India, as shown in Appendix §B.4, suggesting the changes in 2020 not local holidays. (We found a similar event in Thailand, omitted due to space.)

5 RELATED WORK

In this paper, we leverage network measurements to infer changes in daily human activity, and validate our algorithm against possible events due to Covid WFH, given the impact of Covid-19 on our lives. Here we discuss several studies and consider their interactions.

Diurnal Networks and Trends: Diurnal activity and seasonality are common in many time series, including networking. Several well-established mathematical methods exist to extract seasonal

trends [24, 51]. It is well known that network traffic is diurnal, but recent work showed that IP address usage often shows diurnal patterns [72]. We use diurnal address usage to detect human activity, and established tools to extract underlying trends (§2.5).

Covid and Network Traffic: Several groups have reported about how the Internet responded to changes during Covid-19. Ukani et al. studied the network usage of university students at the application level [93]. Facebook reported large traffic increases following lockdown [12]. Another study evaluated traffic changes from an ISP, IXP, and an educational network [33]. Researchers examined the Italian Internet during Covid-19, finding increased variability in latency [17]. ICANN examined the impact of a nationwide lockdown in France on DNS, showing increases in overall DNS traffic [5]. Telefónica analyzed how cellular network usage and performance shifted in UK [59]. Toorn et al. investigated how rDNS entries change due to work-from-home measures [94]. While the above work studies traffic of different kinds, we are the first to study address responsiveness applied to understand real-world events. Our data also provides a global perspective (although non-uniform), rather than that of one service.

Researchers have used Google Trends to correlate public interest in Covid with observed cases [29], goals that are close to ours, but with a very different signal. We study Covid-related changes using the Internet, too, but we consider WFH as inferred from IP address usage without special access to other metrics of traffic.

Active Internet Measurement: Several prior groups have studied the Internet with active probing of some or all of the Internet, often to study address use or outages. USC began whole-Internet censuses in 2006 to evaluate address usage [49]. ZMap [28] and Massscan [42] emphasize scanning speed. Other systems have leveraged active probing to detect outages: Thunderping probes addresses in areas undergoing weather events to look for outages [79]. Trinocular pings millions of networks, inferring outages from Bayesian inference [71]. Chocolatine employs SARIMA models to forecast Internet Background Radiation (IBR) time series to detect outages [45]. It uses data from the UCSD Network Telescope [16]. Richter et al. infer network disruptions from drops in traffic as seen by a major CDN [74]. Disco monitors the bursts of TCP disconnects to detect outages [82]. Dainotti et al. use BGP updates and IBR to study the Internet outages caused by censorship at the country level [23]. Hubble combines active probing with passive BGP monitoring to detect Internet failures. It also identifies network entities that might be the cause [56]. Our work builds on these prior systems for active scanning and reuses data from Trinocular, but with the new algorithms and the new application of detecting human activity.

6 CONCLUSIONS

We have shown that observations of the Internet address responsiveness can detect daily human-activity changes —the first demonstration of inferring large-scale human activity from IP responsiveness, and an important example of using the Internet to understand our world. Our algorithms reconstruct diurnal trends from existing data collected to detect Internet outages, augment it with additional probing, then detect changes in daily IP address usage. We validate the algorithms by studying their components, evaluating randomly selected blocks, verifying observed changes end-to-end, and illustrating news events in multiple locations.

ACKNOWLEDGMENTS

REFERENCES

[1] ANT Project. 2022. ANT Covid-Work-from-Home Datasets. https://ant.isi.edu/datasets/covid/. https://ant.isi.edu/datasets/covid/

[2] APNIC. 2020. Routing Table Report - Japan view. https://mailman.apnic.net/mailing-lists/bgp-stats/archive/2019/10/msg00001.html

[3] APNIC. 2020. Routing Table Report - Japan view. https://mailman.apnic.net/mailing-lists/bgp-stats/archive/2020/01/msg00001.html

[4] APNIC. 2020. Routing Table Report - Japan view. https://mailman.apnic.net/mailing-lists/bgp-stats/archive/2020/04/msg00001.html

[5] Roy Arends. 2020. Analysis of the Effects of COVID-19-Related Lockdowns on IMRS Traffic. *Roy Arends* (Apr. 15 2020). https://www.icann.org/en/system/files/files/octo-008-15apr20-en.pdf

[6] Associated Press. 2020. Timeline: China's COVID-19 outbreak and lockdown of Wuhan. https://abcnews.go.com/Health/wireStory/timeline-chinas-covid-19-outbreak-lockdown-wuhan-75421357.

[7] Guillermo Baltra and John Heidemann. 2020. Improving Coverage of Internet Outage Detection in Sparse Blocks. In *Proceedings of the Passive and Active Measurement Conference*. Springer, Eugene, Oregon, USA.

[8] Guillermo Baltra and John Heidemann. 2021. *What Is The Internet? (Considering Partial Connectivity)*. Technical Report arXiv:2107.11439v2. USC/Information Sciences Institute. https://doi.org/10.48550/arXiv.2107.11439v2

[9] Guillermo P. Baltra. 2023. *Improving network reliability using a formal definition of the Internet core*. Ph. D. Dissertation. University of Southern California, Computer Science Department.

[10] Robert Beverly, Ramakrishnan Durairajan, David Plonka, and Justin P. Rohrer. 2018. In the IP of the Beholder: Strategies for Active IPv6 Topology Discovery. In *Proceedings of the ACM Internet Measurement Conference*. ACM, Boston, Massachusetts, USA, 308–321. https://doi.org/10.1145/3278532.3278559

[11] Timm Böttger, Ghida Ibrahim, and Ben Vallis. 2020. How the Internet reacted to Covid-19—A perspective from Facebook's Edge Network. In *Proceedings of the ACM Internet Measurement Conference*. ACM, Pittsburgh, PA, USA, 34–41. https://doi.org/10.1145/3419394.3423621

[12] Timm Böttger, Ghida Ibrahim, and Ben Vallis. 2020. How the Internet reacted to Covid-19—A perspective from Facebook's Edge Network. In *Proceedings of the ACM Internet Measurement Conference*. ACM, Pittsburgh, PA, USA, 34–41. https://doi.org/10.1145/3419394.3423621

[13] Jon Brodkin. 2020. Netflix, YouTube cut video quality in Europe after pressure from EU official. Ars Technica https://arstechnica.com/tech-policy/2020/03/netflix-and-youtube-cut-streaming-quality-in-europe-to-handle-pandemic/. https://arstechnica.com/tech-policy/2020/03/netflix-and-youtube-cut-streaming-quality-in-europe-to-handle-pandemic/

[14] Xue Cai and John Heidemann. 2010. Understanding Block-level Address Usage in the Visible Internet. In *Proceedings of the ACM SIGCOMM Conference*. ACM, New Delhi, India, 99–110. https://doi.org/10.1145/1851182.1851196

[15] CAIDA. 2007. Archipelago (Ark) Measurement Infrastructure. website https://www.caida.org/projects/ark/. https://www.caida.org/projects/ark/

[16] CAIDA. 2012. Network Telescope. https://www.caida.org/projects/network_telescope/

[17] Massimo Candela, Valerio Luconi, and Alessio Vecchio. 2020. Impact of the COVID-19 pandemic on the Internet latency: A large-scale study. *Computer Networks* 182 (2020), 107495. https://doi.org/10.1016/j.comnet.2020.107495

[18] Tony Cheung, Natalie Wong, and Chan Ho-him. 2020. Coronavirus: 'little, if any, possibility' Hong Kong schools resume fully on April 20, Lam says. South China Morning Post, https://www.scmp.com/news/hong-kong/education/article/3075521/coronavirus-little-if-any-possibility-hong-kong-schools.

[19] Robert B. Cleveland, William S. Cleveland, Jean E. McRae, and Irma Terpenning. 1990. STL: A seasonal-trend decomposition. *Journal of Official Statistics* 6, 1 (1990), 3–73.

[20] Crisis24. 2020. Iran: Natiowide lockdown implemented as over 11,300 COVID-19 cases confirmed March 13 /update 12. https://www.garda.com/crisis24/news-alerts/322811/iran-natiowide-lockdown-implemented-as-over-11300-covid-19-cases-confirmed-march-13-update-12.

[21] Crisis24. 2020. UAE: Three-day lockdown scheduled March 26-29 /update 16. https://www.garda.com/crisis24/news-alerts/326651/uae-three-day-lockdown-scheduled-march-26-29-update-16.

[22] Anthony Cuthbertson. 2020. Coronavirus: France imposes 15-day lockdown and mobilises 100,000 police to enforce restrictions. https://www.independent.co.uk/news/world/europe/coronavirus-france-lockdown-cases-update-covid-19-macron-a9405136.html.

[23] Alberto Dainotti, Claudio Squarcella, Emile Aben, Marco Chiesa, Kimberly C. Claffy, Michele Russo, and Antonio Pescapé. 2011. Analysis of Country-wide Internet Outages Caused by Censorship. In *Proceedings of the ACM Internet Measurement Conference*. ACM, Berlin, Germany, 1–18. https://doi.org/10.1145/2068816.2068818

[24] Alysha M. De Livera, Rob J. Hyndman, and Ralph D. Snyder. 2011. Forecasting time series with complex seasonal patterns using exponential smoothing. *Journal of the American statistical association* 106, 496 (2011), 1513–1527.

[25] Amogh Dhamdhere, David D. Clark, Alexander Gamero-Garrido, Matthew Luckie, Ricky K. P. Mok, Gautam Akiwate, Kabir Gogia, Vaibhav Bajpai, Alex C. Snoeren, and kc claffy. 2018. Inferring Persistent Interdomain Congestion. In *Proceedings of the ACM SIGCOMM Conference*. ACM, Budapest, Hungary, 1–15. https://doi.org/10.1145/3230543.3230549

[26] Marcos Duarte. 2020. detecta: A Python module to detect events in data. https://github.com/demotu/detecta. https://doi.org/10.5281/zenodo.4598962 GitHub repository.

[27] Zakir Durumeric, David Adrian, Ariana Mirian, Michael Bailey, and J. Alex Halderman. 2015. A Search Engine Backed by Internet-Wide Scanning. In *Proceedings of the ACM Conference on Computer and Communications Security*. ACM, Denver, CO, USA, 542–553. https://doi.org/10.1145/2810103.2813703

[28] Zakir Durumeric, Eric Wustrow, and J. Alex Halderman. 2013. ZMap: Fast Internet-wide Scanning and Its Security Applications. In *Proceedings of the USENIX Security Symposium*. USENIX, Washington, DC, USA, 605–620. https://www.usenix.org/system/files/conference/usenixsecurity13/sec13-paper_durumeric.pdf

[29] Maria Effenberger, Andreas Kronbichler, Jae Il Shin, Gert Mayer, Herbert Tilg, and Paul Perco. 2020. Association of the COVID-19 pandemic with Internet search volumes: a Google Trends analysis. *International Journal of Infectious Diseases* 95 (2020), 192–197.

[30] Asma Enayet and John Heidemann. 2022. Internet Outage Detection using Passive Analysis (poster abstract). In *Proceedings of the ACM Internet Measurement Conference*. ACM, Nice, France, 772–773. https://doi.org/10.1145/3517745.3563032

[31] Reid J. Epstein and Kay Nolan. 2020. A Few Thousand Protest Stay-at-Home Order at Wisconsin State Capitol. *New York Times* (Apr. 24 2020). https://www.nytimes.com/2020/04/24/us/politics/coronavirus-protests-madison-wisconsin.html

[32] Anja Feldmann, Oliver Gasser, Franziska Lichtblau, Enric Pujol, Ingmar Poese, Christoph Dietzel, and Daniel Wagner. 2020. The Lockdown Effect: Implications of the COVID-19 Pandemic on Internet Traffic. In *Proceedings of the ACM Internet Measurement Conference*. ACM, Pittsburgh, PA, USA, 1–18. https://doi.org/10.1145/3419394.3423658

[33] Anja Feldmann, Oliver Gasser, Franziska Lichtblau, Enric Pujol, Ingmar Poese, Christoph Dietzel, Daniel Wagner, Matthias Wichtlhuber, Juan Tapiador, Narseo Vallina-Rodriguez, et al. 2021. A year in lockdown: how the waves of COVID-19 impact internet traffic. *Commun. ACM* 64, 7 (2021), 101–108.

[34] Romain Fontugne, Anant Shah, and Kenjiro Cho. 2020. Persistent Last-mile Congestion: Not so Uncommon. In *Proceedings of the ACM Internet Measurement Conference*. ACM, Virtual, 420–427. https://doi.org/10.1145/3419394.3423648

[35] Pawel Foremski, David Plonka, and Arthur Berger. 2016. Entropy/IP: Uncovering Structure in IPv6 Addresses. In *Proceedings of the ACM Internet Measurement Conference*. ACM, Santa Monica, CA, USA, 167–181. https://doi.org/10.1145/2987443.2987445

[36] France 24. 2020. Moscow goes into lockdown, urges other regions to take steps to slow coronavirus. https://www.france24.com/en/20200330-moscow-goes-into-lockdown-urges-other-russian-regions-to-take-measures-to-curb-coronavirus-spread. Online; accessed 29 January 2014.

[37] Oliver Gasser, Quirin Scheitle, Sebastian Gebhard, and Georg Carle. 2016. Scanning the IPv6 Internet: Towards a Comprehensive Hitlist. In *Proceedings of the IFIP International Workshop on Traffic Monitoring and Analysis*. IFIP, Louvain La Neuve, Belgium. http://tma.ifip.org/2016/papers/tma2016-final51.pdf

[38] Jeremy Ginsberg, Matthew H. Mohebbi, Rajan S. Patel, Lynnette Brammer, Mark S. Smolinski, and Larry Brilliant. 2009. Detecting influenza epidemics using search engine query data. *Nature* 457 (Feb. 19 2009), 1012–1014. https://doi.org/10.1038/nature07634

[39] F. Gont. 2014. *A Method for Generating Semantically Opaque Interface Identifiers with IPv6 Stateless Address Autoconfiguration (SLAAC)*. RFC 7217. Internet Request For Comments. https://doi.org/10.17487/RFC7217

[40] F. Gont and T. Chown. 2016. *Network Reconnaissance in IPv6 Networks*. RFC 7707. Internet Request For Comments. https://doi.org/10.17487/RFC7707

[41] Google. 2021. Google IPv6. Web page https://www.google.com/ipv6/. https://www.google.com/intl/en/ipv6/statistics.html

[42] Robert Graham, Paul McMillan, and Dan Tentler. 2014. Mass Scanning the Internet. Presentation at Defcon 22. https://defcon.org/images/defcon-22/dc-22-presentations/Graham-McMillan-Tentler/DEFCON-22-Graham-McMillan-Tentler-Masscaning-the-Internet.pdf

[43] Sarthak Grover, Mi Seon Park, Sam Burnett Srikanth Sundaresan, Hyojoon Kim, and Nick Feamster. 2013. Peeking Behind the NAT: An Empirical Study of Home Networks. In *Proceedings of the ACM Internet Measurement Conference*. ACM, Barcelona, Spain. http://conferences.sigcomm.org/imc/2013/papers/imc061-groverA.pdf

[44] The Guardian. 2020. Belgium enters lockdown over coronavirus crisis – in pictures. https://www.theguardian.com/world/gallery/2020/mar/18/belgium-enters-lockdown-over-coronavirus-crisis-in-pictures.

[45] Andreas Guillot, Romain Fontugne, Philipp Winter, Pascal Merindol, Alistair King, Alberto Dainotti, and Cristel Pelsser. 2019. Chocolatine: Outage Detection for Internet Background Radiation. In *Proceedings of the IFIP International Workshop on Traffic Monitoring and Analysis*. IFIP, Paris, France, 8 pages. https://doi.org/10.23919/TMA.2019.8784607

[46] Hang Guo and John Heidemann. 2018. Detecting ICMP Rate Limiting in the Internet. In *Proceedings of the Passive and Active Measurement Conference*. Springer, Berlin, Germany, to appear.

[47] Fredrik Gustafsson. 2000. *Adaptive Filtering and Change Detection*. Vol. 1. John Wiley & Sons, Inc. https://doi.org/10.1002/0470841613

[48] Mackenzie Haffey, Martin Arlitt, and Carey Williamson. 2018. Modeling, Analysis, and Characterization of Periodic Traffic on a Campus Edge Network. In *Proceedings of the 26th International Symposium on Modelling, Analysis and Simulation of Computer and Telecommunication Systems*. IEEE, Milwaukee, WI, USA. https://doi.org/10.1109/MASCOTS.2018.00025

[49] John Heidemann, Yuri Pradkin, Ramesh Govindan, Christos Papadopoulos, Genevieve Bartlett, and Joseph Bannister. 2008. Census and Survey of the Visible Internet. In *Proceedings of the ACM Internet Measurement Conference*. ACM, Vouliagmeni, Greece, 169–182. https://doi.org/10.1145/1452520.1452542

[50] Morgan Hekking. 2020. COVID-19: Morocco Declares State of Emergency. *Morocco World News* (Mar. 19 2020). https://www.moroccoworldnews.com/2020/03/296213/covid-19-morocco-declares-public-health-emergency https://www.moroccoworldnews.com/2020/03/296213/covid-19-morocco-declares-public-health-emergency.

[51] Rob J Hyndman and George Athanasopoulos. 2018. *Forecasting: principles and practice*. OTexts.

[52] IANA. 2021. IPv4 Address Space Registry. https://www.iana.org/assignments/ipv4-address-space/ipv4-address-space.xhtml

[53] Basileal Imana, Aleksandra Korolova, and John Heidemann. 2021. Institutional Privacy Risks in Sharing DNS Data. In *Proceedings of the Applied Networking Research Workshop*. ACM, Virtual.

[54] UN India. 2020. COVID-19: Lockdown across India, in line with WHO guidance. https://news.un.org/en/story/2020/03/1060132.

[55] Cecilia Kang, Davey Alba, and Adam Satariano. 2020. Surging Traffic Is Slowing Down Our Internet. *New York Times* (Mar. 26 2020). https://www.nytimes.com/2020/03/26/business/coronavirus-internet-traffic-speed.html

[56] Ethan Katz-Bassett, Harsha V. Madhyastha, John P. John, Arvind Krishnamurthy, David Wetherall, and Thomas E. Anderson. 2008. Studying Black Holes in the Internet with Hubble. In *USENIX Symposium on Network Systems Design and Implementation*, Vol. 8. USENIX, 247–262.

[57] Christian Kreibich, Nicholas Weaver, Boris Nechaev, and Vern Paxson. 2010. Netalyzr: Illuminating The Edge Network. In *Proceedings of the ACM Internet Measurement Conference*. ACM, Melbourne, Victoria, Australia, 246–259. http://conferences.sigcomm.org/imc/2010/papers/p1.pdf

[58] W.E. Leland, M.S. Taqqu, W. Willinger, and D.V. Wilson. 1994. On the self-similar nature of Ethernet traffic (extended version). *ACM/IEEE Transactions on Networking* 2, 1 (Feb. 1994), 1–15. http://www.acm.org/pubs/citations/journals/ton/1994-2-1/p1-leland/

[59] Andra Lutu, Diego Perino, Marcelo Bagnulo, Enrique Frias-Martinez, and Javad Khangosstar. 2020. A Characterization of the COVID-19 Pandemic Impact on a Mobile Network Operator Traffic. In *Proceedings of the ACM Internet Measurement Conference*. ACM, Pittsburgh, PA, USA, 19–33. https://doi.org/10.1145/3419394.3423655

[60] Por Valéria Martins. 2020. Casos de pacientes com coronavírus sobe para 197 em SC e governo prorroga quarentena. https://g1.globo.com/sc/santa-catarina/noticia/2020/03/29/casos-de-pacientes-com-coronavirus-sobe-para-197-em-sc-e-governo-prorroga-quarentena.ghtml.

[61] Felipe Mata, Piotr Żuraniewski, Michel Mandjes, and Marco Mellia. 2014. Anomaly detection in diurnal data. *Computer Networks* 60 (2014), 187–200. https://doi.org/10.1016/j.bjp.2013.11.011

[62] Maxmind. 2020. GeoLite City. Web page http://dev.maxmind.com/geoip/geolite. http://dev.maxmind.com/geoip/geolite

[63] Gertjan Medema, Leo Heijnen, Goffe Elsinga, Ronald Italiaander, and Anke Brouwer. 2020. Presence of SARS-Coronavirus-2 RNA in Sewage and Correlation with Reported COVID-19 Prevalence in the Early Stage of the Epidemic

in The Netherlands. *Environmental Science and Technology Letters* 7 (May 2020), 511–516. https://doi.org/10.1021/acs.estlett.0c00357

[64] Giovane C. M. Moura, Carlos Gañán an Qasim Lone, Payam Poursaied, Hadi Asghari, and Michel van Eeten. 2015. How Dynamic is the ISPs Address Space? Towards Internet-Wide DHCP Churn Estimation. In *Proceedings of the IFIP Networking*. IFIP, 1–9. https://doi.org/10.1109/IFIPNetworking.2015.7145335

[65] El Mundo. 2020. Pedro Sánchez anuncia el estado de alarma para frenar el coronavirus 24 horas antes de aprobarlo. https://www.elmundo.es/espana/2020/03/13/5e6b844e21efa0dd258b45a5.html.

[66] Austin Murdock, Frank Li, Paul Bramsen, Zakir Durumeric, and Vern Paxson. 2017. Target Generation for Internet-wide IPv6 Scanning. In *Proceedings of the ACM Internet Measurement Conference*. ACM, San Diego, CA, USA, 242–253. https://doi.org/10.1145/3131365.3131405

[67] Ramakrishna Padmanabhan, Amogh Dhamdhere, Emile Aben, kc claffy, and Neil Spring. 2016. Reasons Dynamic Addresses Change. In *Proceedings of the ACM Internet Measurement Conference*. ACM, Santa Monica, CA, USA, 183–198. https://doi.org/10.1145/2987443.2987461

[68] Ramakrishna Padmanabhan, John P. Rula, Philipp Richter, Stephen D. Strowes, and Alberto Dainotti. 2020. DynamIPs: Analyzing address assignment practices in IPv4 and IPv6. In *Proceedings of the ACM Conference on Emerging Networking Experiments and Technologies*. ACM, Barcelona, Spain, 55–70. https://doi.org/10.1145/3386367.3431314

[69] Ramakrishna Padmanabhan, Aaron Schulman, Dave Levin, and Neil Spring. 2019. Residential Links Under the Weather. In *Proceedings of the ACM SIGCOMM Conference*. ACM, Beijing, China, 145–158. https://doi.org/10.1145/3341302.3342084

[70] ANT Project. 2013. ANT Project Outage Datasets. https://ant.isi.edu/datasets/outage/. https://ant.isi.edu/datasets/outage/

[71] Lin Quan, John Heidemann, and Yuri Pradkin. 2013. Trinocular: Understanding Internet Reliability Through Adaptive Probing. In *Proceedings of the ACM SIGCOMM Conference*. ACM, Hong Kong, China, 255–266. https://doi.org/10.1145/2486001.2486017

[72] Lin Quan, John Heidemann, and Yuri Pradkin. 2014. When the Internet Sleeps: Correlating Diurnal Networks With External Factors. In *Proceedings of the ACM Internet Measurement Conference*. ACM, Vancouver, BC, Canada, 87–100. https://doi.org/10.1145/2663716.2663721

[73] Reuters. 2020. Venezuela's to implement nationwide quarantine as coronavirus cases rise to 33. https://www.reuters.com/article/us-health-coronavirus-venezuela-maduro/venezuelas-to-implement-nationwide-quarantine-as-coronavirus-cases-rise-to-33-idUSKBN214015.

[74] Philipp Richter, Ramakrishna Padmanabhan, Neil Spring, Arthur Berger, and David Clark. 2018. Advancing the Art of Internet Edge Outage Detection. In *Proceedings of the ACM Internet Measurement Conference*. ACM, Boston, Massachusetts, USA, 350–363. https://doi.org/10.1145/3278532.3278563

[75] Philipp Richter, Georgios Smaragdakis, David Plonka, and Arthur Berger. 2016. Beyond Counting: New Perspectives on the Active IPv4 Address Space. In *Proceedings of the ACM Internet Measurement Conference*. ACM, Santa Monica, CA, USA, 135–149. https://doi.org/10.1145/2987443.2987473

[76] Philipp Richter, Florian Wohlfart, Narseo Vallina-Rodriguez, Mark Allman, Randy Bush, Anja Feldmann, Christian Kreibich, Nicholas Weaver, and Vern Paxson. 2016. A Multi-perspective Analysis of Carrier-Grade NAT Deployment. In *Proceedings of the ACM Internet Measurement Conference*. ACM, Santa Monica, CA, USA. https://doi.org/10.1145/2987443.2987474

[77] Lauren Robel. 2020. A Letter to Hoosiers. Student communications https://provost.indiana.edu/statements/covid/for-students/march-19.html. https://provost.indiana.edu/statements/covid/for-students/march-19.html

[78] Sarah Schafer. 1998. With Capital in Panic, Pizza Deliveries Soar. *The Washington Post* (Dec. 19 1998), D1. https://www.washingtonpost.com/wp-srv/politics/special/clinton/stories/pizza121998.htm

[79] Aaron Schulman and Neil Spring. 2011. Pingin' in the Rain. In *Proceedings of the ACM Internet Measurement Conference*. ACM, Berlin, Germany, 19–25. https://doi.org/10.1145/2068816.2068819

[80] Skipper Seabold and Josef Perktold. 2010. Statsmodels: Econometric and statistical modeling with Python. In *Proceedings of the 9th Python in Science Conference*, Vol. 57. Austin, TX, scipy.org, 61.

[81] M. Zubair Shafiq, Lusheng Ji, Alex X. Liu, and Jia Wang. 2011. Characterizing and Modeling Internet Traffic Dynamics of Cellular Devices. In *Proceedings of the ACM SIGMETRICS*. ACM, San Jose, CA, USA, 305–316. https://doi.org/10.1145/1993744.1993776

[82] Anant Shah, Romain Fontugne, Emile Aben, Cristel Pelsser, and Randy Bush. 2017. Disco: Fast, good, and cheap outage detection. In *2017 Network Traffic Measurement and Analysis Conference (TMA)*. IEEE, 1–9.

[83] Natalie Sims and Barbara Kasprzyk-Hordern. 2020. Future perspectives of wastewater-based epidemiology: monitoring infectious disease spread and resistance to the community level. *Environment international* 139 (2020), 105689.

[84] Radiotelevizija Slovenija. 2020. Staršem 50 odstotkov plače, varstvo za nujno potrebne poklice. https://www.rtvslo.si/zdravje/novi-koronavirus/starsem-50-odstotkov-place-varstvo-za-nujno-potrebne-poklice/516908.

[85] Heather Stewart, Rowena Mason, and Vikram Dodd. 2020. Boris Johnson orders UK lockdown to be enforced by police. https://www.theguardian.com/world/2020/mar/23/boris-johnson-orders-uk-lockdown-to-be-enforced-by-police.

[86] Erica Stutz, Yuri Pradkin, Xiao Song, and John Heidemann. 2021. ANT Evaluation of COVID-19 Internet Downtrends. https://covid.ant.isi.edu/. https://covid.ant.isi.edu/

[87] Erica Stutz, Yuri Pradkin, Xiao Song, and John Heidemann. 2021. Visualizing Internet Measurements of Covid-19 Work-from-Home. In *Proceedings of the National Symposium for NSF REU Research in Data Science, Systems, and Security (REU 2021 Symposium)*. IEEE, Virtual Workshop, 5633–5638.

[88] Erbil Sulaymaniyah. 2020. Iraq's KRG eases coronavirus lockdown after two months. https://www.aa.com.tr/en/middle-east/iraqs-krg-eases-coronavirus-lockdown-after-two-months/1838231.

[89] Eric Sylvers and Giovanni Legorano. 2020. As Virus Spreads, Italy Locks Down Country. https://www.wsj.com/articles/italy-bolsters-quarantine-checks-after-initial-lockdown-confusion-11583756737.

[90] Markus Söder. 2020. Lockdown was started in Freiburg, Baden-Württemberg and Bavaria on 20 March 2020. Two days later, it was expanded to the whole of Germany. https://pbs.twimg.com/media/ETjc738WoAI5zAt?format=jpg&name=large.

[91] Sangeeta Tanwar. 2020. Delhi chief minister seeks Indian Army's help after riots claim 20 lives over two days. *Quartz India* (Feb. 25 2020). https://qz.com/india/1808434/arvind-kejriwal-wants-curfew-army-to-quell-delhi-riots/

[92] New Straits Times. 2020. Covid-19: Movement Control Order imposed with only essential sectors operating. https://www.nst.com.my/news/nation/2020/03/575177/covid-19-movement-control-order-imposed-only-essential-sectors-operating.

[93] Alisha Ukani, Ariana Mirian, and Alex C. Snoeren. 2021. Locked-in during Lock-down: Undergraduate Life on the Internet in a Pandemic. In *Proceedings of the 21st ACM Internet Measurement Conference (IMC '21)*. Association for Computing Machinery, New York, NY, USA, 480–486. https://doi.org/10.1145/3487552.3487828

[94] Olivier van der Toorn, Raffaele Sommese, Anna Sperotto, Roland van Rijswijk-Deij, and Mattijs Jonker. 2022. Saving Brian's Privacy: the Perils of Privacy Exposure through Reverse DNS. *CoRR* abs/2202.01160 (2022). arXiv:2202.01160 https://arxiv.org/abs/2202.01160

[95] Deutsche Welle. 2020. Coronavirus: What are the lockdown measures across Europe? https://www.dw.com/en/coronavirus-what-are-the-lockdown-measures-across-europe/a-52905137.

[96] C. Williamson, E. Halepovic, Hongxia Sun, and Yujing Wu. 2005. Characterization of CDMA2000 cellular data network traffic. In *Proceedings of the 30th IEEE International Conference on Local Computer Networks*. IEEE, Sydney, NSW, Australia. https://doi.org/10.1109/LCN.2005.37

[97] Eric Wustrow, Manish Karir, Michael Bailey, Farnam Jahanian, and Geoff Huston. 2010. Internet Background Radiation Revisited. In *Proceedings of the 10th ACM SIGCOMM Conference on Internet Measurement* (Melbourne, Australia) *(IMC '10)*. Association for Computing Machinery, New York, NY, USA, 62–74. https://doi.org/10.1145/1879141.1879149

[98] Yinglian Xie, Fang Yu, Kannan Achan, Eliot Gillum, Moises Goldszmidt, and Ted Wobber. 2007. How Dynamic are IP Addresses?. In *Proceedings of the ACM SIGCOMM Conference*. ACM, Kyoto, Japan, 301–312. https://doi.org/10.1145/1282380.1282415

A RESEARCH ETHICS AND DATA AVAILABILITY

In developing a new measurement technique, we must consider the potential new risks it creates for individuals and organizations. Our overall goal is to identify human activity. Our general way to minimize risk is to focus on aggregate activity and avoid the identification of individuals through a combination of technical and policy methods.

Risks: The primary risk to individuals is that data may expose the activity of specific users—work schedules of individuals may be sensitive. We avoid this risk by separating what we learn about IP addresses from knowledge of specific individuals. We do not have any the knowledge of which individuals use which IP addresses, so our data does not, by itself, pose any risk to individuals.

Of course, *other* datasets associate IP addresses with individuals. ISPs and organizations may track user-to-IP mapping for accountability. Combining such mapping data with our data might pose a risk. We minimize this risk by aggregating data by /24 prefixes early in our processing pipeline and handling pre-aggregated data with largely automated procedures. Our analysis requires specific IP addresses only through the reconstruction phase (§2.3). Finally, we commit not to join pre-aggregated data with other data sources that risk de-anonymization.

Beyond individuals, WFH activity may be sensitive to organizations [53]. For example, increased deliveries correlate with longer work and may indicate unusual events [78]. In some countries and regions, Covid response has become politicized; its absence may be seen as supportive or critical of government policies. While protecting the privacy of individuals is important, the reputation of organizations or regions must be balanced with the public's need to understand the choices people make.

In addition to privacy concerns, the measurement traffic we use places a small burden on the studied networks. Fortunately, about 6/7ths of the measurement data used in this paper was collected for an ongoing measurement study (Trinocular [71]). The only *new* data we collect are the additional observations in §2.8. However, even if we take responsibility for *all* measurements (including pre-existing measurements), the original Trinocular work [71] showed that its cost is quite minimal: each observer adds less than 1% to 2010 background radiation for targeted blocks [97]. With scanning (both benign and malicious) far more prevalent today than in 2010, this relative estimate would certainly be smaller today.

Benefits: The benefits of our work are to provide a new method of identifying trends in human activity on a global scale by reanalyzing existing data. The Covid pandemic is an ongoing global health crisis resulting in millions of deaths with broad social and economic impacts over the last two years. We believe that our analysis can provide a new perspective on actual human activity, thereby contributing to discussions about public health response. Although measurements of the Internet have their own limitations, we see it as providing a valuable complement to traditional tools to understand public health, such as surveys, institutional reporting, and wastewater monitoring.

In our view, these benefits outweigh the risks.

Data collection: Most of our analysis is new evaluation of the existing datasets listed in Table 6, although we also are taking additional data (§2.8). Although some risk is created by new information available through our analysis, the underlying data and therefore the potential of such risk is not new.

Data distribution: We are committed to providing the results of our data to the research community and no charge. However, to ensure that researchers do not create additional privacy risks, we distribute data under terms-of-use that forbids de-anonymization and redistribution.

IRB review: Our work was reviewed by our university's Institutional Review Board and because it does not identify individuals, it was classified as non-human-subjects research (USC #UP-20-00909).

Datasets: Table 6 lists all datasets used in this paper.

B CASE STUDY OF SPECIFIC BLOCKS

We use Figure 1 as a running example in §2 to show our methodology. It was one of many that we examined when developing our approach. We next review additional blocks to provide more representatives of changes that we observed.

abbr.	dataset name	start	duration
2023q1-c	internet_outage_adaptive_a51c-20230101	2023-01-01	12 weeks
2023q2-c	internet_outage_adaptive_a52c-20230401	2023-04-01	12 weeks
2020q1-e	internet_outage_adaptive_a39e-20200101	2020-01-01	12 weeks
2020q2-e	internet_outage_adaptive_a40e-20200401	2020-04-01	12 weeks
2023q1-e	internet_outage_adaptive_a51e-20230101	2023-01-01	12 weeks
2023q2-e	internet_outage_adaptive_a52e-20230401	2023-04-01	12 weeks
2023q1-g	internet_outage_adaptive_a51g-20230101	2023-01-01	12 weeks
2023q2-g	internet_outage_adaptive_a52g-20230401	2023-04-01	12 weeks
2020q1-j	internet_outage_adaptive_a39j-20200101	2020-01-01	12 weeks
2020q2-j	internet_outage_adaptive_a40j-20200401	2020-04-01	12 weeks
2020q1-n	internet_outage_adaptive_a39n-20200101	2020-01-01	12 weeks
2020q2-n	internet_outage_adaptive_a40n-20200401	2020-04-01	12 weeks
2023q1-n	internet_outage_adaptive_a51n-20230101	2023-01-01	12 weeks
2023q2-n	internet_outage_adaptive_a52n-20230401	2023-04-01	12 weeks
2019q4-w	internet_outage_adaptive_a38w-20191001	2019-10-01	12 weeks
2020q1-w	internet_outage_adaptive_a39w-20200101	2020-01-01	12 weeks
2020q2-w	internet_outage_adaptive_a40w-20200401	2020-04-01	12 weeks
2023q1-w	internet_outage_adaptive_a51w-20230101	2023-01-01	12 weeks
2023q2-w	internet_outage_adaptive_a52w-20230401	2023-04-01	12 weeks
2020it89-w	internet_address_survey_reprobing_it89w-20200219	2020-02-19	2 weeks

Table 6: Existing, publicly available datasets used in this paper, from [70]. Letter indicates observer's location: c: Colorado data from Ft. Collins; e: ISI-East, near Washington, DC; g: Greece, at Athens U. of Economics in Business; j: Japan, Keio University, near Tokyo; n: Netherlands, near Utrecht; w: ISI-West, Los Angeles.
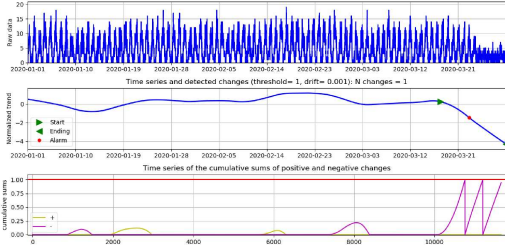
(a) The anon. block with only diurnal activity.
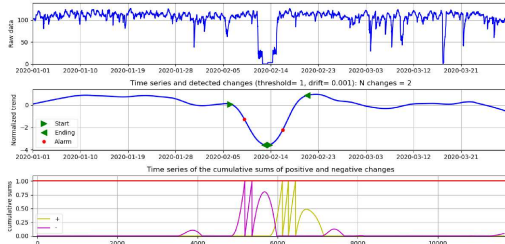
(b) The anon. block with a non Covid-related change.

Figure 11: Two representative change-sensitive blocks.

B.1 Detection in Two Additional Blocks

We first show a diurnal block that appears to have a Covid-related change. In Figure 11a we see active addresses change from 0 to 20 over each 24 hours, a trend that occurs all days of the week, including weekends. The diurnal activity disappears on 2020-03-20, suggesting a Covid-related lockdown. This block is in the U.A.E., so this event roughly matches news reports (see §3.7).

Figure 11b shows another block that is change-sensitive, with a small but detectable diurnal swing. This block shows a small

decrease in trend in the last few days of March, but not enough to trigger detection. It also shows a large change in mid-February, with active address dropping from around 100 to 0. We believe this event corresponds to a network outage or ISP-based reassignment of users to another address block. The pair of a downward trend followed up an upward detection shown in the bottom bar is typical of this kind of event. This example is consistent with the pair of downward and upward trends that occur over many blocks in Beijing on 2002-04-15 and -18, shown in Figure 9b.

B.2 A Pre-Covid VPN

We next consider a /24 block (128.125.52.0/24) that is part of USC's VPN (Figure 15). We initially determined it was VPN based on reverse DNS addresses, and then later confirmed this use with USC network operators.

Figure 15a shows the number of active addresses over time. We see that after 10 weeks of steady use, the address usage drops off significantly, just as WFH begins. This outcome seems backwards from what one would expect —VPN usage should go up with WFH. USC network operators explained that they shifted the campus VPN to a newer, larger address space because of an anticipated increase in use. Thus use of address space went down because use shifted to another block.

Figure 15b confirms that the usage change is found with change-point detection. This block is classified as change-sensitive block. We observe the number of active IP addresses has a significant drop around 2020-03-15 based on Figure 15a and the upper bar chart of Figure 15b. The change point detected around 2020-03-15 reflects ground truth that WFH begins at USC.

Our detection algorithms find this block, but tracking migration to different blocks is outside the scope of this paper.

B.3 Beijing in 2023q1

Figure 12 presents changes in Wuhan and Beijing in the first quarter of 2023. We see a significant peak around 2023-01-20 in Beijing. According to Holiday Calendar, Spring Festival in China started from 2023-01-22 and lasted until early February. This suggests that the peak is related to people leaving workplace and staying at home during Spring Festival.

B.4 New Delhi in 2023q1

Figure 13 shows that there is no distinguishable peak in New Delhi in 2023q1, whereas we saw a large change in late March in 2020q1.

C RECONSTRUCTION CASE STUDIES

We next examine good and difficult sample blocks to help understand factors that affect the reconstruction quality. Figure 4 shows two blocks, comparing the survey's ground truth (the dark blue line) against our reconstruction (the light orange line).

Reconstruction in the top block is accurate; Pearson's correlation coefficient is 0.89 and a scan time is 3300 s (about an hour). Qualitatively, the shape matches, with reconstruction and working ours both showing daily peaks matching working hours, sharp changes at the start of each day, and flat activity between workdays. The main difference is the maximum number of active, with reconstruction 9% lower than truth. This shortfall is because Trinocular stops probing after a success, so discovery of new addresses is slow. However, the reconstruction preserves change sensitivity.
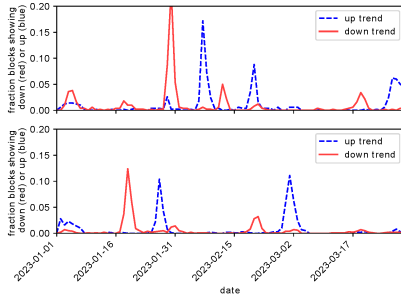
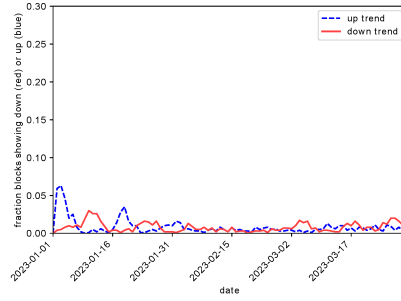**Figure 12: *Changes for Wuhan (top) and Beijing (bottom), 2023q1.**

Figure 13: *Changes for (28N, 76E: New Delhi), 2023q1
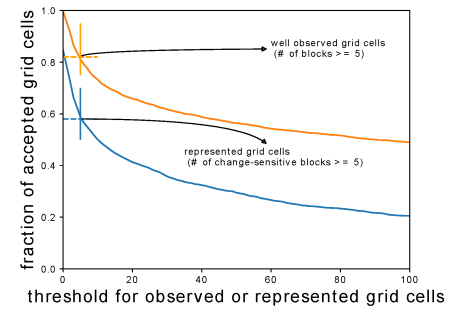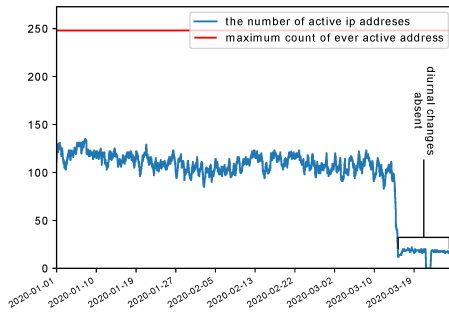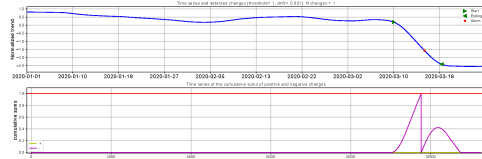
Figure 14: The CDF of number of blocks in gridcells.

(a) Active addresses over 3 months (input data).

(b) STL trend with annotations (top) and CUSUM sums (bottom).

Figure 15: A VPN block (128.125.52.0/24) and detection.

The block in the lower figure shows a greater challenge for reconstruction. This block is heavily used (120 to 160 active addresses), and it sees a large daily shift, with consistent changes every day of the week. With many active addresses, a full scan requires 8 hours and reconstruction (orange) lags truth (blue). We see the low-pass effects of reconstruction, spreading out some of the true activity, flattening the peaks and raising the valleys. The correlation coefficient is 0.40.

Both blocks show imperfect reconstruction, but reconstruction is sufficient for change-sensitivity and these blocks are used in WFH detection. They motivate additional probing and reasons blocks may be misclassified (Table 3).

D THRESHOLDS FOR GEOGRAPHIC COVERAGE

In §3.5 we examined geographic coverage, and we required thresholds of at least 5 change-sensitive blocks for represented gridcell, and 5 ping-responsive blocks as an observed gridcell. We select these values to avoid false-positives due to noise from non-WFH changes that can occur in single blocks.

Figure 14 shows how sensitive coverage is to varying these thresholds. The blue line represents number of change-sensitive blocks in gridcells. The orange line represents the number of blocks in gridcells. We see similar results for geographic coverage for most small values of 3 or more. Weighted values are very insensitive to these thresholds because the majority of blocks are in gridcells with good observability or representation.

E INDIANA ON 2020-03-15

To understand applicability of our approach in North America we explored WFH events in the United States through our website [86].

Our website supports examination of the underlying blocks. We can see that 36 blocks in Indiana University (AS87 and AS27198) were detected as WFH on 2020-03-15. This data corresponds with the beginning of spring break (Friday, 2020-03-13) followed by remote learning beginning on 2020-03-19 [77].

This example shows the use of our algorithms and website to discover an event unknown to us. It also shows the role of universities for having change-sensitive networks. Universities often have large IPv4 allocations (as Autonomous System 87, IU was an early adopter) and so are able to use public IP addresses for dynamic use.